Spatial distribution, migration, and population structure of North Sea rays

Jan Jaap Poos, Timo Staeudle, Eleanor Greenway and Jurgen Batsleer

WAGENINGEN
UNIVERSITY & RESEARCH

Spatial distribution, migration, and population structure of North Sea rays

Jan Jaap Poos[1], Timo Staeudle[1], Eleanor Greenway[1] and Jurgen Batsleer[2]

1 Aquaculture and Fisheries Group, Wageningen University and Research

2 Wageningen Marine Research, Wageningen University and Research

Europees Fonds voor Maritieme Zaken en Visserij

This research project was carried out by Wageningen University and Research and subsidized by the ministry of Agriculture, Nature and Food Quality.

This report can be downloaded from: https://doi.org/10.18174/632935.

Cover foto: Reindert Nijland

Wageningen, June 2023.

Summary

Little is known about the migratory behaviour of sharks and rays in the Greater North Sea ecoregion. While several ray stocks were widespread in the early 20th century, the population declines resulted in a reduced distribution area of most rays, with the east coast of the UK and the Eastern English Channel being the hotspots for abundance for most larger species. The recovery in abundance also results in a larger distribution area, including parts of the Dutch EEZ. The question is how these different areas are connected in terms of migration and population genetics.

To study migration of rays, we tagged 224 specimens of three ray species; spotted ray (*Raja montagui*), blonde ray (*Raja brachyura*), and thornback ray (*Raja clavata*). This tagging was done using CEFAS G5 Data Storage Tags (DSTs). Each tag was attached to an individual ray at the basis of the tail. To ensure minimum effect of the tag on the ray, a protocol was developed to attach the tag to a ray, with the goal of having a procedure for attachment that was as short as possible, and with minimum effect on the ray.

DSTs measure and store temperature and depth of the individual that they are attached to, The G5 DSTs used in this study can be programmed to detach from the animal ('pop-off') after a set time. Because the DSTs are slightly buoyant, they will float to the surface and be taken to land by currents and winds. When the tags were found by fishers on live rays, or by beach combers, the temperature and depth records can be downloaded from the tag and analyzed. These temperature and depth profiles can subsequently be used to reconstruct the migration pattern of the individual rays. Because the pop-off time for the deployed tags has not been reached, we now have a limited set of returned tags: 30 tags were returned, with the majority being found on beaches. Most returned tags were retuned within 6 months after release.

Of the 30 tags which were returned, 7 were reported by fishers and therefore both capture and recapture locations are known, shown in figure 4. These 'traditional' mark and recaptures give preliminary insights into skate movements in the North Sea and English Channel: While some tags were recaptured close to the release positions, others were found far from the release positions. One tag was released north of the Dutch Wadden Sea and was recaptured off the English coast. In some cases, the tags were recaptured in different ICES divisions from their release position.

Mapping spatial distributions of ray populations using Integrated Nested Laplace Approximation (INLA) on research vessel survey data showed the changes in spatial distributions of *Raja clavata* and *R. brachyura*. Data was used from 1988, when the survey coverage of the Eastern English Channel was complete, to 2022. Data from three different surveys were used, estimating potential differences in catchability between the surveys in the model. Three size classes were distinguished in the model, with boundaries between classes being based on the length at which rays become vulnerable to the fishery, and length at first maturity. Both species increased in overall population abundance, with higher abundances in the eastern part of the southern North Sea. The range of spatial correlation in abundances was slightly smaller for *R. brachyura* compared to *R. clavata*.

A large number of rays from different locations in the North Sea was genotyped, and combined with earlier genotypes from the species. Genotyping was done by means of "Genotyping by Sequencing" and by means of an Illumina SNP chip. No clear population genetic structure was found within the North Sea for any of the species, while structure did exist outside of the North Sea for *R. clavata*.

To conclude, there are clear increases observed in the abundances of the demersal elasmobranch stocks in the Southern part of the Greater North Sea ecoregion. As a result, more rays are observed in the Dutch part of the North Sea. Meanwhile, no clear population genetic structure was observed for the stocks. This could be explained by the migration that is observed from tagging data, even with the limited set of tags that has yet been returned. The tags that have been returned show clear diel vertical migration patterns in all species. The number of returned tags is expected to increase substantially over the next two years, as more pop-off dates are reached. Such a full set of tag data can be used to reconstruct annual migration patterns, as was demonstrated by the tags analysed in this study.

Contents

Introduction

Elasmobranchs (i.e. sharks, skates and rays) play an important role as predators in marine ecosystems (Dulvy et al., 2000; Heithaus et al., 2008). Their specific life-history traits, i.e. being long-lived, showing slow growth, late sexual maturity and producing a small number of young per year, make them vulnerable to fishing, pollution and changes in essential habitats, especially spawning and nursery areas (Frisk et al., 2001; Amelot et al., 2021). As a result, the abundance of several skates and rays in the North Sea declined in the 20th century (Sguotti et al., 2016). Improving the population size of elasmobranchs in the North Sea is an important environmental objective under the EU Marine Strategy Framework Directive. Since 2010 a recovery in the abundances of some species is observed.

Little is known about the migratory behaviour of sharks and rays in the Greater North Sea ecoregion. While several ray stocks were widespread in the early 20th century, the population declines resulted in a reduced distribution area of most rays (Walker and Heessen, 1996; Sguotti et al., 2016), with the east coast of the UK and the Eastern English Channel being the hotspots for abundance for most larger species. The recovery in abundance also results in a larger distribution area, including parts of the Dutch EEZ. The question is how these different areas are connected in terms of migration and population genetics. Specifically, the role of the North Sea and the Dutch coastal zone for the life cycle of sharks and rays, and in the factors that affect their spatial dynamics and distribution. This can be studied in two ways:

1. Identifying migration patterns using Data Storage Tags (DSTs), shedding light on the effect of individual migration behaviour on the spatial distribution of the population.

2. Mapping spatial distributions of populations using research vessel survey data, supported by genetic data to map possible sub populations.

Many elasmobranchs display home ranges, migration patterns and site fidelity (Carrier et al., 2012) where daily, seasonal and ontogenetic changes may also be observed in habitat use and distribution patterns (Bird et al., 2020; Brevé et al., 2020; Grubbs, 2010; Thorburn et al., 2019). Spatial segregation by size and/or sex is observed in some elasmobranch populations with regards to habitat preference and behaviour (Griffiths et al., 2020; Hunter et al., 2006; Sims et al., 2001). Such differences in spatial distribution may lead to increased vulnerability of particular life stages such as juveniles and reproductively active females (Heupel et al., 2007; Martin et al., 2010). Ecologically important areas include nursery grounds and oviposition (egg-laying) sites, as well as potential sites for large aggregations (e.g., for mating or feeding). In the North Sea, such areas are currently unknown for many species. However, the Thames Estuary is a known area of importance for thornback ray *R. clavata* and may also be ecologically important for other demersal elasmobranchs such as spotted ray *R. montagui* and blonde ray *R. brachyura* for which distribution and migration patterns are poorly known (Ellis et al., 2005; ICES, 2020). These three species were selected at the start of the project

With tag data, fine-scale diel vertical migration of *R. brachyura* and *R. montagui*, in the North Sea, can be identified. Distribution and migration of fish are mostly described in long-term horizontal movements but less for daily vertical movements in the water column. Data storage tags (DSTs) allow the study of diel vertical migration (DVM). DVMs are observed in many pelagic species including elasmobranchs (Andrews et al., 2009; Humphries et al., 2016; Shepard et al., 2006). Marine animals exhibit DVMs in order to avoid predators or to track prey which is ultimately caused by changes in light levels (Mehner, 2012; Mehner et al., 2007). DVMs usually display daily movements from deeper depths during daylight hours to shallower depths at night. DVMs of benthic predators are unlike those of pelagic predators and usually represent offshore-inshore movements, where individuals move from deeper waters to shallower coastal areas (Humphries et al., 2017; Hunter et al., 2005). DVMs in benthic elasmobranchs was thought to be unlikely due to their morphological evolution but this behaviour has been observed in catsharks (*Scyliorhinus canicula*) (Sims et al., 2006), and *R. clavata* (Humphries et al., 2017).

Research vessel survey information has been collected for rays in the Greater North Sea ecosystem has been collected for over three decades (Amelot et al., 2021). These data are publicly available in a database called DATRAS, hosted by the International Council for the Exploration of the Sea. INLA Models (Rue et al.,

2009) can be used to account for spatiotemporal variability in survey data, through spatial and temporal correlation structure in latent variables (Thorson and Minto, 2015). Several research vessel surveys fishing for demersal species take place in the Greater North Sea: The International Bottom Trawl Survey (IBTS), the Beam Trawl Survey (BTS), and the Channel Ground Fish Survey (CGFS). The IBTS and BTS surveys consist of fishing hauls done by different countries using different vessels, with some standardisation of the gears within surveys. To account for the differences in gears among surveys, a survey effect needs to included.

Genetic marker research allows revealing population structure in the rays int the North Sea. Population structure is the presence of a systematic difference in genetic variation between subpopulations. Such differences in allele frequencies between subpopulations indicate presence of non-random mating, e.g. because of distance or barriers. Identifying the genetic variation can be done using single nucleotide polymorphisms (SNPs) in large numbers of samples.

The ultimate aim of the project was to bridge the main gaps in our knowledge on the distribution and migration of demersal rays. Three species were selected for our research: *Raja clavata*, *R. brachyura*, and *R. montagui*. These are the most commonly observed ray species in the southern North Sea. The project ran for two years and was funded by the Ministry of Agriculture, Nature and Food Quality as part of a larger project "Bridging knowledge gaps for sharks and rays".

Methods

Tagging

Since 3rd August 2021 until present (22/05/2023), individuals were caught opportunistically from the Dutch and Belgium Bottom Trawl Survey (BTS), French and Dutch International Bottom Trawl survey (IBTS) and commercial vessels (TX3, SL45, MDV2 and SCH135) in the North Sea, English Channel and Dutch Coast. Fishing gears used to capture and tag rays include beam trawl, twin rig and flyshoot. *R. brachyura*, *R. montagui*, and *R. clavata* were tagged with CFL G5 pDSTs (Cefas Technology, UK). G5 pDSTs are 71.5 mm in length x 30 mm in diameter and weigh 30 grams. These pDSTs log temperature (accuracy 0.1 °C, resolution 0.03 °C) and pressure (accuracy 1%, resolution 0.04%) every 10 seconds. The pDSTs are programmed to separate or 'pop-off' from the individual after 12 - 24 months at liberty on the 1st August 2023, 1st July 2024, and 1st July 2025.

A €25 euro reward and a free T-shirt was advertised to those who reported a tag. However due to the unexpected number of tags returned in the first year, the reward changed to either a €25 reward or a T-shirt. 'Tag finders' receive a package which contained a pre-labelled box, with which to return the tag, the information flyer designed by the Dutch Elasmobranch Society, and several small posters to raise awareness of the tagging project. All text was translated into five languages: Dutch, English, French, German and Danish. Any sending costs were also reimbursed.

Before skates are tagged, vitality scores were given to each individual based on reflex responses and any injuries. Only skates with the highest vitality scores were tagged to ensure the highest chance of survival. Due to the weight and size of the tag, only individuals larger than 50 cm were be tagged. Tags wee surgically attached using a stainless-steel wire cradle joined at two attachment sites at the base of the tail caudal to the pelvic girdle (Figure 1). Pre-prepared cradles with two plastic Peterson discs and a rubber plate kept the cradle in place with two pointed ends of wire. The cradle was passed dorso-ventrally through the base of the tail, with the spine medial to each puncture site. A second rubber plate and two additional plastic Peterson discs are placed onto the length of the wires on the ventral side of the tail. The cradle was secured by turning two or more rounds into the length of wire, keeping ~1 cm gap between the tag and the tail, and the remaining wire was removed. This method of 'cradle attachment' was designed to reduce any potential behavioural effects and reduce stress to the animal during the tagging procedure, which lasted between 1 min 2 seconds and 4 minutes. The base of the tail was chosen for the tag attachment site as it results in symmetrical drag and reduced interference with muscle movements compared to tag attachment on the wings. The potential effects of drag were partially negated due to the positive buoyancy of the tags, from its floatation collar, and this reduces the potential impact on the behaviour of the individual. The size of the tags restricts the size of individuals which could be tagged (>50 cm). Our data therefore consisted mostly of mature individuals.

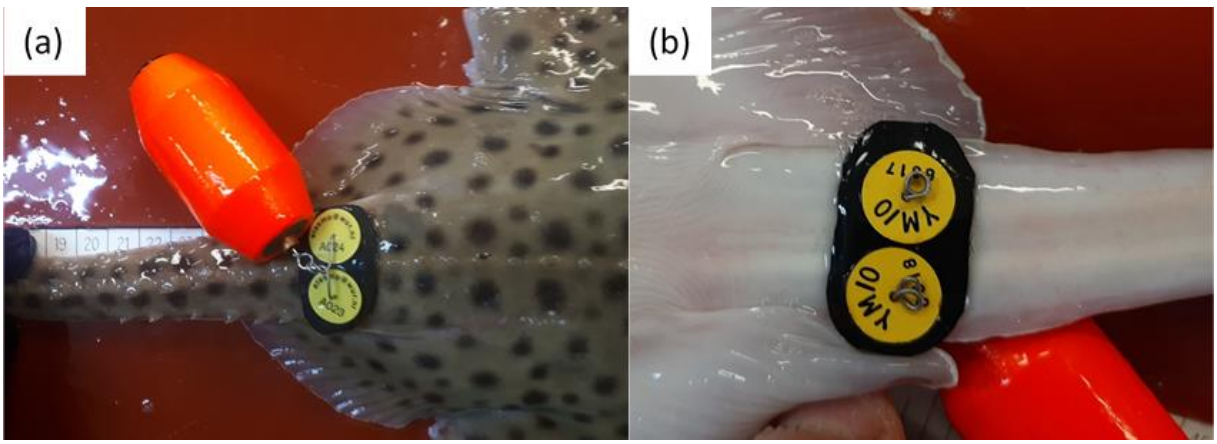

Figure 1. Placement of the 'pop-off' data storage tag at the base of the tail caudal to the pelvic girdle. The spine is medial to the two attachment sites of the stainless-steel wire cradle. The cradle is held in place with two Peterson discs and a rubber plate on the dorsal (a) and ventral side (b) of the individual.

Time series data collected from the tags are in the process of being analysed using the tidal location method (Hunter et al., 2003), in collaboration with colleagues from CEFFAS. Data collected from the pDSTs are compared with the tidal database, (the North Sea tidal clock) then geolocations of individual tags can be estimated during the time at liberty. Changes in swimming behaviour from on-bottom to mid water are determined by depth changes of ≥ 3m. Geolocations are eliminated if derived positions vary >10m or derived temperatures vary >1°C compared to recorded depth and temperature data. Maximum swimming speed is set at one body length per second to identify plausible geolocations (Hunter et al., 2003; Hunter et al., 2005). High swimming speeds (~ 2 body lengths per second) or 'jetting' may also be observed for brief periods but are energetically costly and therefore unsustainable (Di Santo et al., 2017; Greenway et al., 2016). Table 1 shows an ethogram of observed behaviours, some of which are detected in the tag data.

Spatial abundance using survey data

INLA Models (Rue et al., 2009) were used to account for spatiotemporal variability in survey data, through spatial and temporal correlation structure in latent variables (Thorson and Minto, 2015). Here, long-term survey data spanning more than 30 years from the Database of Trawl surveys (DATRAS) were used to estimate total and exploitation length class biomass indices for *Raja clavata* and *R. brachyura* across ICES areas 3a, 4, and 7d from 1988-2021.

Exchange data of three scientific trawl surveys were downloaded from the ICES DATRAS database (ICES, 2021) for the period 1988-2021: International Bottom Trawl Survey (NS-IBTS) for Quarter 1 and 3, the Beam Trawl Survey (NS-BTS) for Quarter 3 and the Channel Groundfish Survey (FR-CGFS) for Quarter 4. 1988 was chosen for the starting period of the analysis since it was the first year for which data from the English Channel was available. For each haul, catch per haul was calculated and aggregated into 3 length class categories based on exploitation status and length-at-maturity curves. The exploitation threshold was set to >= 50cm for both species, with individuals <50cm classified as unexploited.

The threshold for maturity classification was different between the two species: for *R. clavata* it was defined as 71cm, with immature size class defined as <71cm and mature size class as ≥71cm, as previous studies estimated North Sea specific L50 of 68 cm for males (Walker, 1999) and 74 cm for females (McCully et al.,

Table 1. Ethogram of behaviours as described by Greenway et al. (2016).

Behaviour	Description	Definition
Resting	Horizontal Resting	Ventral side touching bottom of the tank, no or very little movement
	Burying	Oscillating outer body rapidly to move sand onto body
	Moving tail	Moving tail side to side while keeping rest of the body still.
Locomotory	Crawling	Ventrally moving using pelvic fins to push sand along the bottom of the tank
	Swimming	Moving through the water without touching the water surface or floor of the tank
	Jetting	When an individual quickly propels itself to move away from a stimulus
	Digging	Using snout and fins to move substrate
	Shake	Quickly moving body (leading with the head/snout) side to side. This can be done whilst vertical, horizontal or during a swimming behaviour
Thigmotaxis	Vertical Resting	Resting ventral side against the wall of the tank, no or very little movement
	Vertical Swimming	Swimming whist ventrally touching the wall of the tank
	Vertical Burying	Oscillating outer body whilst ventral side is against the wall of the tank
	Bopping	When resting vertically, the individual repeatedly moves up and down the side of the tank
Stereotypical Behaviour	Surface Breaking Behaviour	Swimming with head/snout above the water's surface*
	Spiralling	Swimming around a central point horizontally and vertically in a back flip motion

2012). For *R. brachyura*, the maturity threshold was defined as 81cm , with immature size class defined as <81 cm and mature size class as ≥81 cm, as previous studies estimated North Sea specific L50 of 78 cm for males and 83 cm for females (McCully et al., 2012).

Fished surface area was calculated for hauls based on wingspread times distance for NS-IBTS, beam size times distance for FR-CGFS and NS-BTS. Missing wingspread or beam size was extrapolated for hauls in the NS-IBTS and FR-CGFS if missing, whereas missing haul distances were extrapolated for hauls in the NS-BTS.

The mixed-effect model in INLA was defined as follows:

$$C_{it} \sim NB(\mu_{it}, k)$$

$$E(C_{it}) = \mu_{it}$$

$$\text{var}(C_{it}) = \mu_{it} + \frac{\mu_{it}^2}{k}$$

$$\log(\mu_{it}) = Intercept + Survey + Size\ class\ + offset(logSurfaceSweptAreakm2) + \alpha_{tm} + \beta_{dm} + \nu_{it}$$

$$\alpha_t \sim N(0, \rho_\alpha)$$

$$\beta_{dm} = \beta_{d-1,m} + \eta_{d,m}, \quad \eta_{dm} = N(0, \frac{1}{\rho_{\eta_{d,m}}})$$

$$\nu_{it} = \rho_t \times \nu_{i,t-1} + \upsilon_{i,t}$$

$$\upsilon_{i,t} \sim GMRF(0, \Sigma)$$

where C_{it} represents catch per haul i in year (t), assuming negative binomial distribution with an estimated mean (μ_{it}) and estimated shape parameter (k). The mean is modelled using a number of covariates; Survey has three levels, one for each of the surveys. 3 exploitability-maturity size classes in the model were explored: unexploited immatures (<50cm) represented by $m = 0$, exploited immatures (>= 50cm & < 71cm) represented by m = 1, exploited matures (>= 71cm) represented by $m = 2$. The offset term incorporates the log of the swept area for each haul as the estimated mean count increases linearly with swept area. Year was modelled as independent and identically distributed (iid) random effect with mean equal to 0 and an estimated precision ρ_α to comply with the assumption for stock assessment model that estimates for Years are independent of each other.

The spatio-temporal component of the model ν_{it}, is defined as combination of a spatially autoregressive gaussian random field (υ_{ti}) with a dependence on the distance between locations (i), and a temporally autoregressive gaussian random field, where ρ determines the temporal correlation between hauls at locations (i). The temporal field was modelled with 9 temporal nodes from 1988-2021 due to high computational costs that rapidly arise in continuous space (see the "Big n problem"; (Jona Lasinio et al., 2012)). An space-discretizing mesh with 930 vertices was designed based on regularly shaped triangles.

For the spatio-temporal models the additional covariates EUNIS2019C (or including substrate or EUNIS2019D_substrate as covariates) did not yet result in successful model fits.

Models of increasing complexity were compared using the deviance information criterion (DIC), Watanabe–Akaike information criterion (WAIC), and the Condition Predictive Ordination (CPO). The DIC and WAIC measure the compromise between fit and parsimony. The CPO can be summarised by the mean logarithmic CPO (LCPO) (Roos and Held, 2011) to assess the predictive power of the model as a "leave one out" cross-validation index (Pennino et al., 2013; Lezama-Ochoa et al., 2020). Lower DIC and WAIC suggest better model performance.

Population genetic structure

Genotype collection

Sampling of tissues needed for genotyping was done at various fish auctions in the Netherlands, during surveys with research vessels, aboard trips where discards were collected, and with the help of skippers in the discards sampling program. In the latter sampling, rays were brought whole to Wageningen Marine Research (WMR) and tissue samples were then taken by WMR personnel.

To ensure proper sampling, short protocols were created that could be given to researchers. Using these protocols, tissue samples were taken as consistently as possible. In addition to these protocols, samplers were also given pre-filled forms on which the position, sex, height, and weight of samples were recorded. Samplers were given 200 to 300 Eppendorf tubes pre-filled with 96% alcohol. In these, the tissue samples were collected and stored at -20 °C.

A second category of tissues was another group of samples made available by the University of Groningen. These were tissue samples of thornback ray collected for research in the period 2000-2010. These samples provided insight into changes in the genetic composition of ray populations, within and outside the North Sea and these tissue samples were therefore sent for genotyping.

Genotyping for thornback ray was done using an Infinium® XT iSelect96 SNP array. This SNP ("Single-nucleotide Polymorphism") array was developed by Labogena (www.labogena.fr) for the genotyping of thornback ray. The SNP array contains 9120 potential SNPs for thornback ray. These SNPS were determined using RADseq (Restriction site Associated DNA sequencing) for fin clips from 225 individuals from coastal zones of the Northeast Atlantic and the Mediterranean Sea, described in Marandel et al. (2020).

Genotyping for blonde ray was done using Genotyping by sequencing (GBS; Elshire et al. 2011). Genotyping was done by Diversity Arrays Technology (www.diversityarrays.com). In the project, low density (LD) sequencing was chosen, using DArTseqTM as described in Kilian et al. (2012). Samples were sequenced (single read) using an Illumina® HiSeq® 2500, with approximately 0.5 million sequences determined for each individual.

Genotyping for spotted ray (*Raja montagui*) was done using Genotyping by sequencing (GBS; Elshire et al. 2011). Genotyping was performed by Diversity Arrays Technology (www.diversityarrays.com). In the project, DArTseq Medium density sequencing was chosen, using DArTseqTM as described in Kilian et al. (2012). Samples were sequences (single read) using an Illumina Hiseq2500/Novaseq6000, with approximately 1.2 million sequences determined for each individual.

For all species, about 1% of the total individuals were sent as duplicates for genotyping. A comparison of the duplicate genotyping gave insight into the consistency of the genotyping method.

Quality control of genotypes

The genotypes found were subjected to quality control to remove sources of error or bias in genotyping. In this quality control, SNPs and samples that did not meet a number of criteria were removed stepwise.

For *Raja clavata*, first, misidentified samples were detected and removed by investigating the clustering of samples, given sample and loci call rates, against control samples of *Raja brachyura* and *Raja montagui*. Next, non-scoring loci and monomorphic loci were removed. This was followed by retaining only samples with a call rate threshold ≥0.98, and loci with a call rate threshold ≥0.95 and a minor allele frequency threshold ≥0.05. Unintentional replicates were identified using CKMRsim (v0.1.1.999, Anderson, 2022) with assumed error model of 0.005 and the maximum allowed number of mismatching genotypes between pairs set to 10%. Of each putative replicate pair, the individual with the higher call rate was retained. Putative sex-linked SNPs were detected and removed based on the heterozygote excess in one sex (Trenkel et al. 2020). For any duplicated SNP pair identified, determined based on being within 50 nucleotides of each other during the SNP array development, only SNP with the higher call rate was retained. A random SNP was removed from any SNP pair identified with pairwise linkage disequilibrium (R2 > 0.1). First-

order(parent-offpsring: PO; full-sibling: FS) and second-order(half-sibling: HS) kinship pairs were identified using CKMRsim with assumed and true genotyping error model of 0.005 and 10,000 simulated related kinship pairs based on the observed allele frequencies of SNPs in Hardy-Weinberg Equilibrium. One individual of each related pair was removed from the dataset.

For *Raja brachyura*, misidentified samples were detected and removed by investigating the clustering of samples, given sample and loci call rates, against control samples of *Raja clavata* and *Raja montagui*. Next, non-scoring loci and monomorphic loci were removed. This was followed by retaining only samples with a call rate threshold ≥0.85, and loci with a call rate threshold ≥0.95 and a minor allele frequency threshold ≥0.05. Unintentional replicates were identified using CKMRsim (v0.1.1.999, Anderson, 2022) with assumed genotyping error model of 0.005 and the maximum allowed number of mismatching genotypes between pairs set to 10%. Of each putative replicate pair, the individual with the higher call rate was retained. Putative sex-linked SNPs were detected and removed based on the heterozygote excess in one sex (Trenkel et al. 2020). A random SNP was removed from any SNP pair identified with pairwise linkage disequilibrium (R2>0.1).

For *Raja montagui,* misidentified samples were detected and removed by investigating the clustering of samples, given sample and loci call rates, against control samples of *Raja clavata* and *Raja brachyura*. Next, non-scoring loci and monomorphic loci were removed. This was followed by retaining loci with a reproducibility score ≥0.99 and call rate ≥0.95. Secondaries, multiple SNP loci within a provided DArT fragment, were removed and only loci with read depth ≥5 and ≤50 were retained. Next, samples with a call rate threshold ≥0.95, and loci a minor allele frequency threshold ≥0.05 were retained. Unintentional replicates were identified using CKMRsim (v0.1.1.999, Anderson, 2022) with assumed genotyping error estimated at 0.0087 using Tiger (Bresadola et al. 2020) across intentional replicates and the maximum allowed number of mismatching genotypes between pairs set to 10%. Putative sex-linked SNPs were detected and removed based on the heterozygote excess in one sex (Trenkel et al. 2020). A random SNP was removed from any pair identified with pairwise linkage disequilibrium (R2>0.8). First-order(parent-offpsring: PO; full-sibling: FS) and second-order(half-sibling: HS) kinship pairs were identified using CKMRsim with assumed estimated at 0.0085 using Tiger (Bresadola et al. 2020) across intentional replicates and 10,000 simulated related kinship pairs based on the observed allele frequencies of SNPs in Hardy-Weinberg Equilibrium. One individual of each related pair was removed from the dataset.

Population structure

The population genetic structure of the available genotypes was investigated for *R. clavata*, *R. brachyura*, and *R. montagui*. For *R. brachyura*, genotypes were available from the North Sea and Celtic Seas, with the majority of the samples coming from the North Sea. For *R. montagui*, samples were available from the North Sea and Celtic Seas, with the majority of the samples coming from the North Sea. For *R. clavata*, samples were available from across Western Europe, using genotypes collected in the INNORAYS project, genotypes collected in this project, and genotypes collected by IFREMER in the Bay of Biscay. These genotypes from the IFREMER samples were determined using the same SNP array used for the project. Therefore, they could be used directly to determine population structure in a wider range than just the North Sea.

The population structure in these samples was determined using two approaches. First, Spatial population structure was assed using a Discriminant Analysis of Principal Components (DAPC; Jombart et al., 2010) using the R package adegenet (v 2.1.7). DAPCs were performed with prior grouping of individuals based on ICES Ecoregion, ICES divisions, and statistical rectangles. Furthermore, 1 DAPC was performed with de Novo grouping of individuals based on evaluated number of clusters (K) identified with the find.clusters() function. For RJC DAPC 1/3 of available principal components were used, whereas for RJM and RJH all available principal components were used. The optimal number of clusters was evaluated using the Bayesian information criterion (BIC), the difference in BIC between different clusters, and the slope of the differences. For each DAPC, the optimal number of PCs to use in the DAPC was determined using the optim.a.score() function to prevent overfitting (Miller et al., 2020). Missing data was not replaced with mean allele frequencies.

Second, admixture analysis was done using the R package LEA (v3.6.0), which uses Sparse Nonnegative Matrix Factorization (SNMF) to estimate individual admixture coefficients from the genotypic matrix to determine de novo genetic clusters. It assumes K ancestral populations and provides least-squares estimates of ancestry proportions rather than maximum likelihood estimates (Frichot et al., 2014). Ten repetitions for each number of K (ranging from K=1 to K=10) were performed and cross-entropy criterions calculated to assess the most likely value of K.

Results

Tagging

As of the 20nd June 2023, a total of 224 skates were tagged using the G5 DSTs. Skates of varying lengths were tagged in all species, with fewer individuals from the larger size categories. All tags were deployed on individuals larger than 50 cm. The size distribution of the tagged individuals is clearly affected by the asymptotic size of the species: *Raja clavata* and *R. brachyura* are the two bigger species, with tagged individuals up to 90 cm. *R. montagui* is the smaller of the three species. With tagged individuals up to 65 cm (Figure 2). Meanwhile the sex difference in asymptotic length can also be observed in the tagging size distributions: females grow larger than males, and the largest tagged individuals are indeed females.

Of the 224 tagged individuals, 37 tags were reported where 30 tags were returned. The return rate of the tags up to the present was thus 13.4%. Of the returned tags, 27 have usable data. It should be noted that all tags recovered at this time are before the programmed 'pop-off' day, this denotes that skates were either caught and retained by fishers (n = 7), died at liberty (n = 15) or the tag broke from the attachment pin (n = 8).

The release locations were spread over the Eastern English Channel, and the Southern and Central North Sea, with a substantial part of the release locations being on the Dutch Continental Shelf (Figure 3). Tags were either reported by fishers or by the general public who found tags during beach sightings (Figure 3).

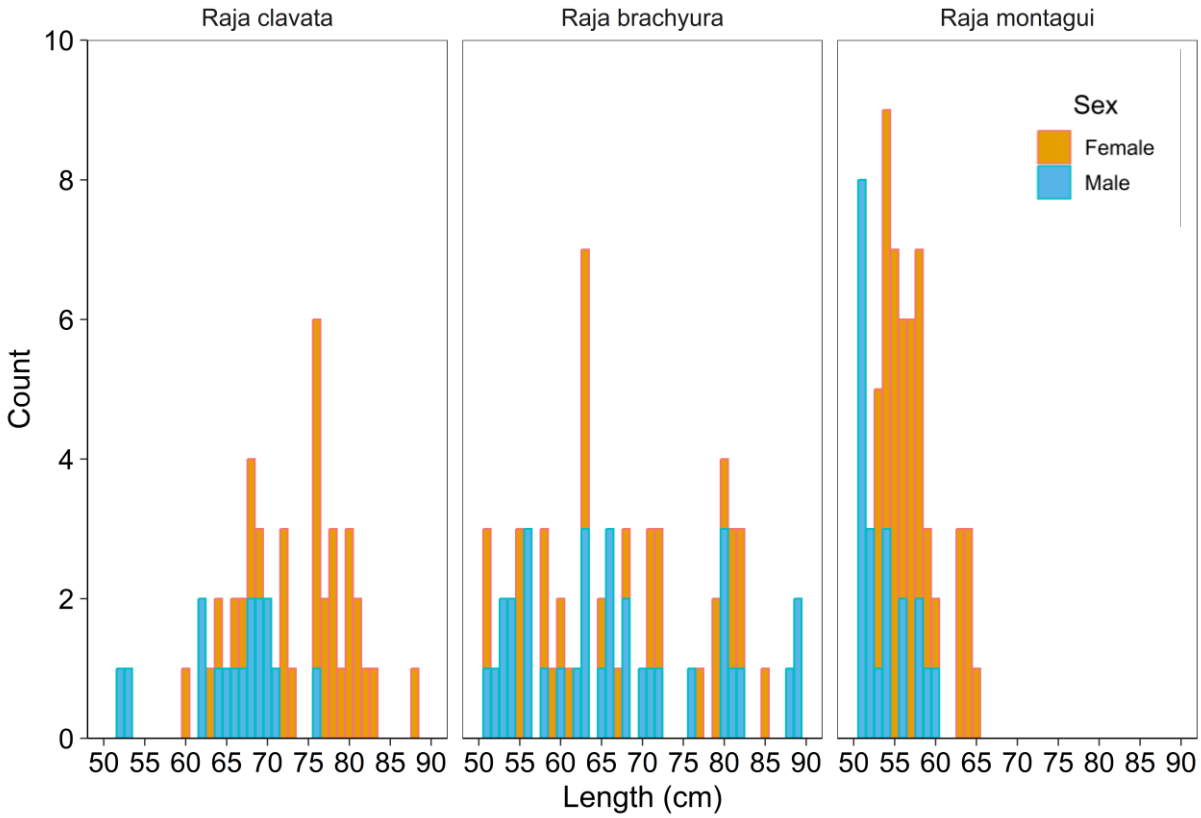

Figure 2. Length distribution of tagged individuals for Raja clavata, Raja brachyura, and Raja montagui.

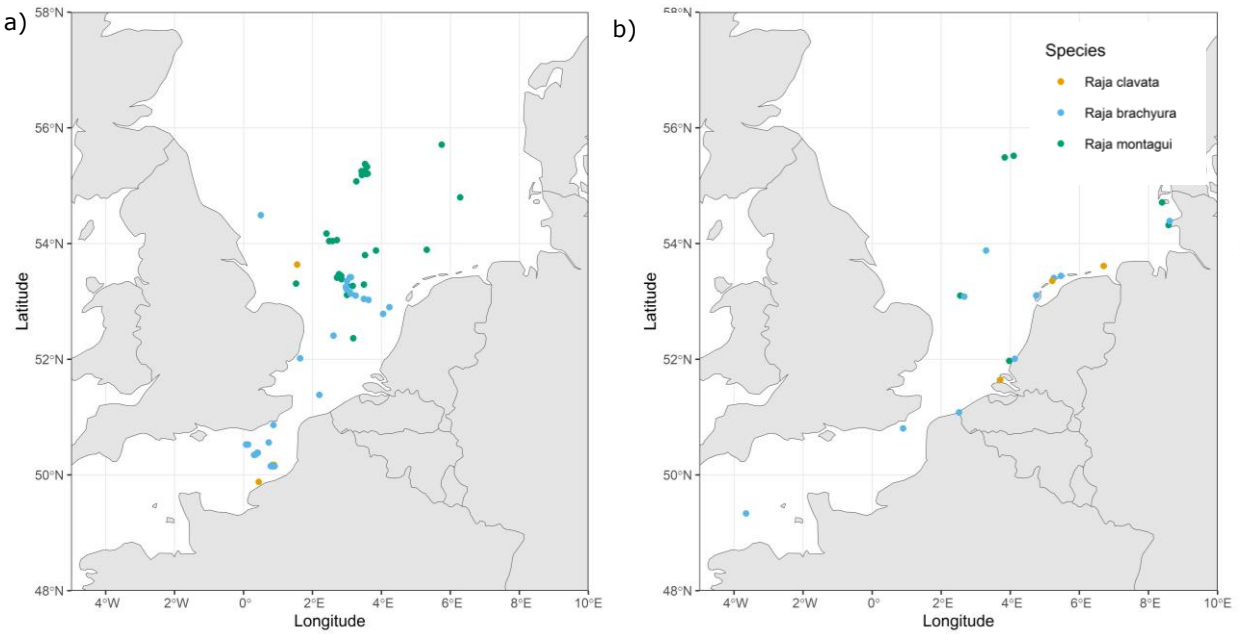

Figure 3. Current a) tagging locations from commercial and survey vessels and b) tag recovery locations from commercial vessels and beach sightings for each species *Raja clavata*, *Raja brachyura* and *Raja montagui*.

Tags were at liberty from 13 to 392 days starting from date of tag deployment (date initial capture and release of the tagged individual) until date of reporting. Note: date of reporting may vary to actual date of recovery (Figure 5). These data show that tagging effort occurred all year round, and all tag data recovered (until May 2023) expands across all seasons in the year.

Of the 30 tags which were returned, 7 were reported by fishers and therefore both capture and recapture locations are known, shown in figure 4. These 'traditional' mark and recaptures give preliminary insights into skate movements in the North Sea and English Channel: While some tags were recaptured close to the release positions, others were found far from the release positions. One tag was released north of the Dutch Wadden Sea and was recaptured off the English coast. In some cases, the tags were recaptured in different ICES divisions from their release position.

In order to determine geolocations, and therefore migration routes, the tidal location method was used. Ongoing collaborations with colleagues at CEFAS will result in migration tracks from individuals at liberty for greater than three months. Figure 6 shows an example of a migration track resulting from the tidal location method for a female *R. montagui* 51 cm in length, tag ID A18029. This individual was recaptured by a fisher also shown in Figure 4. Migration tracks were produced by produced by David Righton from CEFAS.

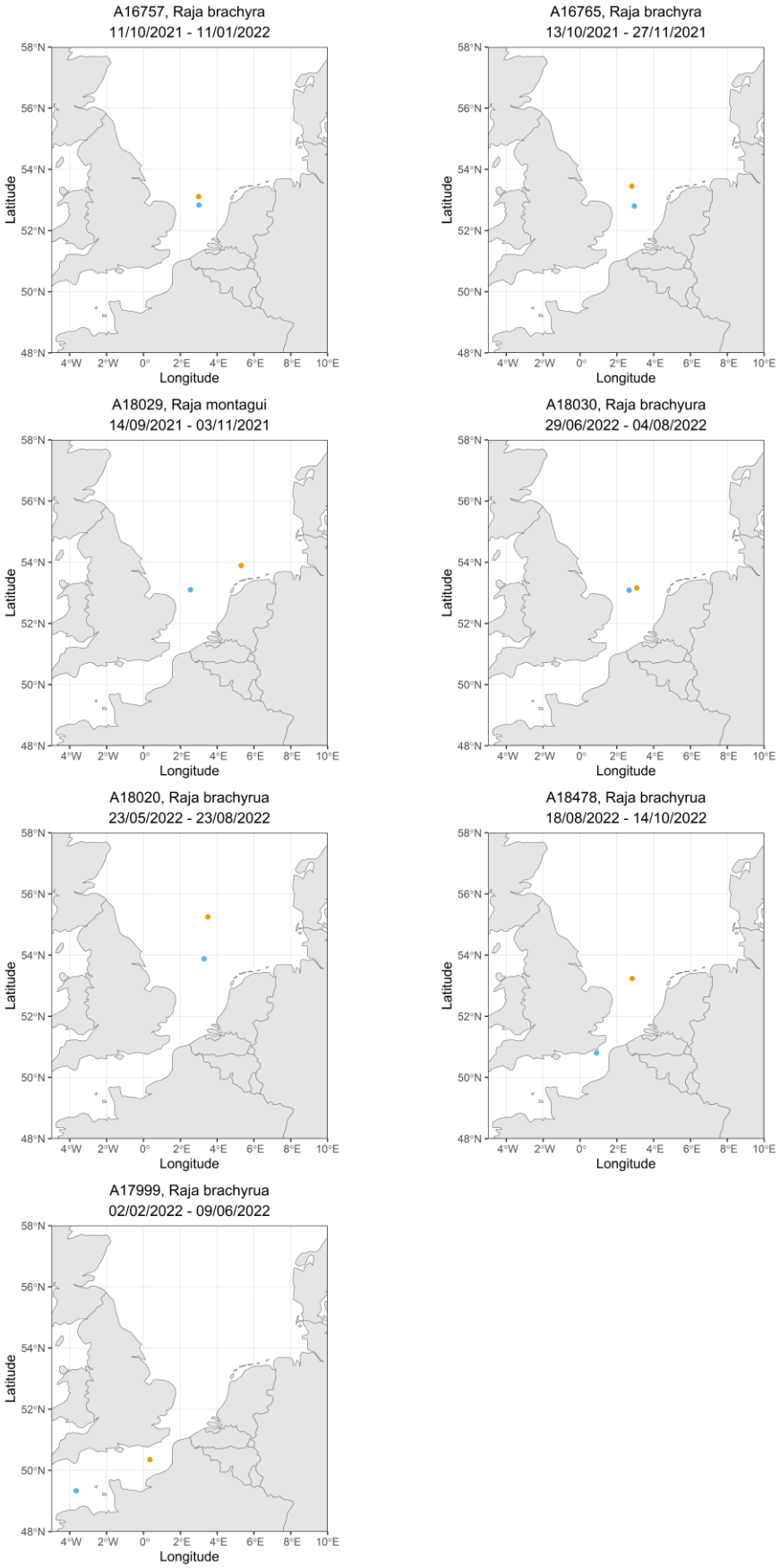

Figure 4. Initial tag locations with known recapture locations and dates for Raja brachyura and Raja. montagui. Where ■ denotes the initial tagging location and ■ denotes recaptured locations from fishers.

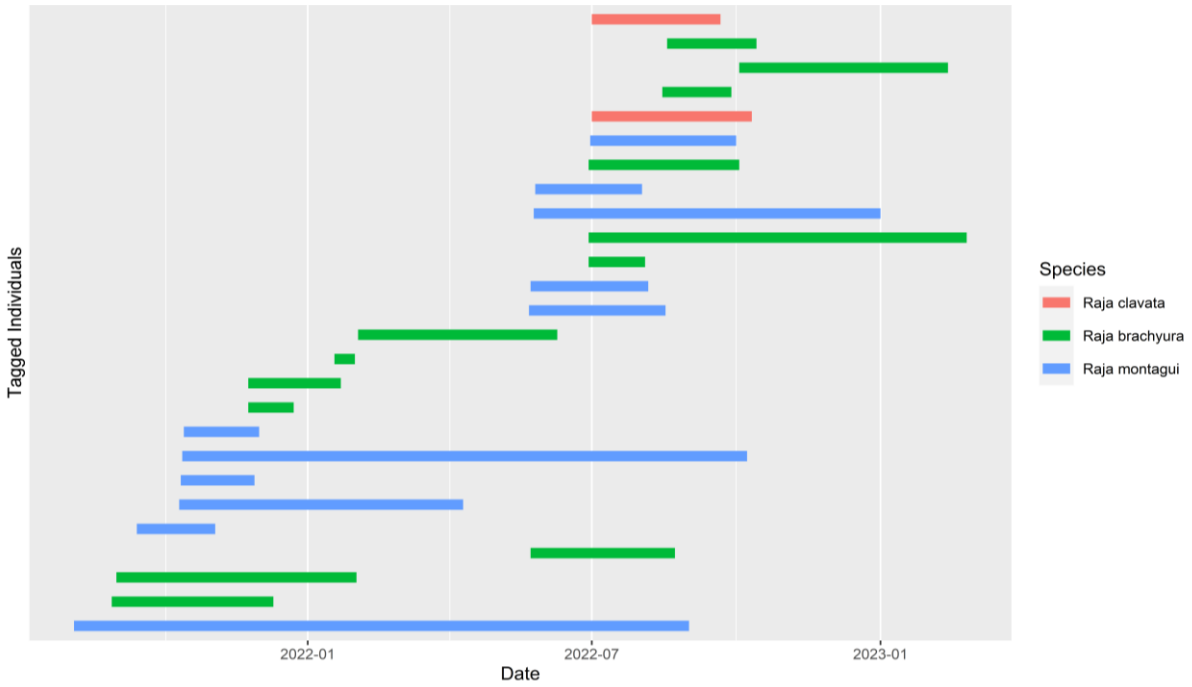

Figure 5. All recovered tags showing the length of time at liberty for each species; Raja clavata (n = 2), Raja brachyura (n = 16), and Raja montagui (n = 12).

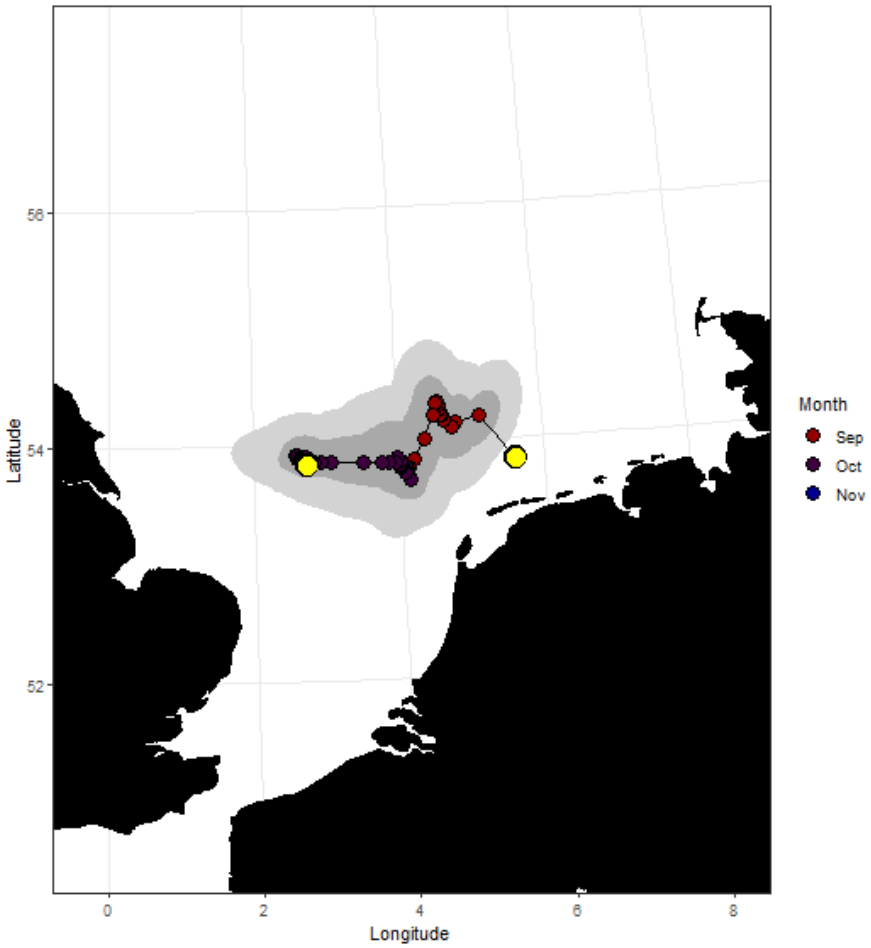

Figure 6. Example of geolocations determined from tag data using the tidal location methods, combined with water temperature, for tag ID A18029; a female R. montagui 50 cm in length. The yellow markers indicate the release and recapture positions. Markers in between indicate migration between these markers, as determined by the tidal location model. Produced by David Righton from CEFAS.

Diel vertical migrations and habitat use

Daily patterns in activity and depth use can also be observed from the tag data. Figure 7 shows observations in depth use in one day (16/09/2021) of a female *R. montagui* 50 cm in length. The data shows on a given day the skate exhibits more swimming behaviour during night-time hours (between 19:00 and 07:00) and generally on the sea floor during day-time hours (between 07:00 and 19:00). The heatmap (figure 8) shows the variance in depth over the entire time at liberty where darker colours denote higher variances in depth i.e. more swimming behaviour, and the lighter colours denotes lower variances in depth i.e. crawling or resting. These data show that this skate consistently shows this pattern in behaviour, where the individual is swimming during night-time hours and on the sea floor during day-time hours.

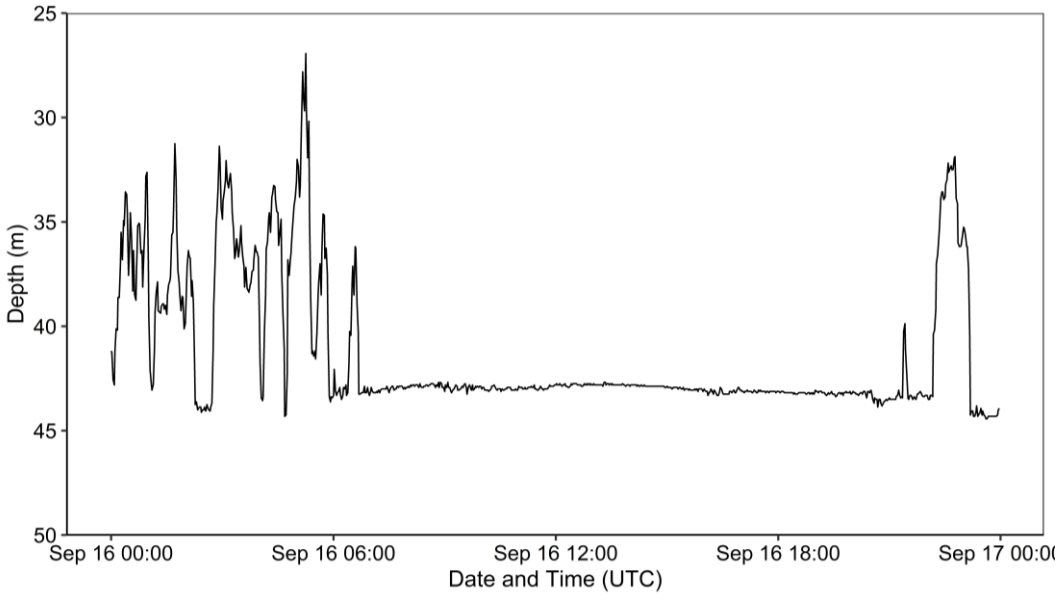

Figure 7. Observations in depth use on the 16th of September 2021 from a female R. montagui 51 cm in length. Tag no: A18029.

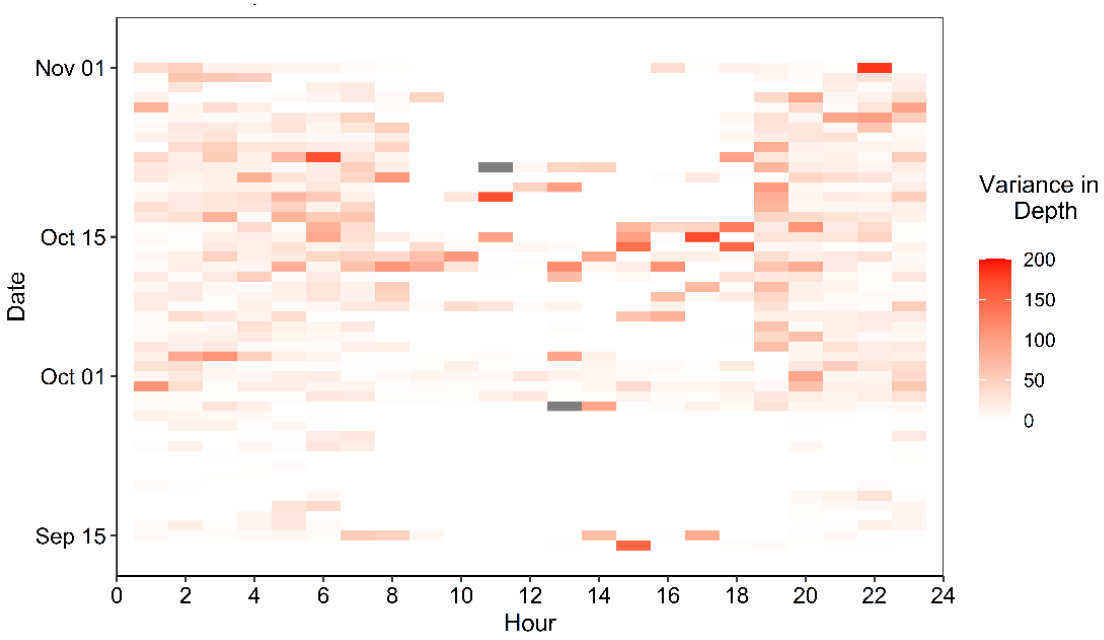

Figure 8. A heatmap showing the variance in depth use during time at liberty (14/09/2021 to 02/11/ 2021), where lower variances in depth are generally observed between 08:00 and 19:00 from a female R. montagui 51 cm in length. Tag no: A18029.

Daily patterns in behaviour were assigned to times of day (dawn, day, dusk and night) to observe potential correlations between time of day and behavioural patterns. Figure 9 shows the same data shown in figure 7 (depth use in one day at liberty, 16/09/2021, of a female *R. montagui* 51 cm in length), where different colours represent different times of the day. The data shows that swimming activity diminishes during dawn hours and commences again during dusk hours. This suggests that daily patterns of activity were contingent on the time of day.

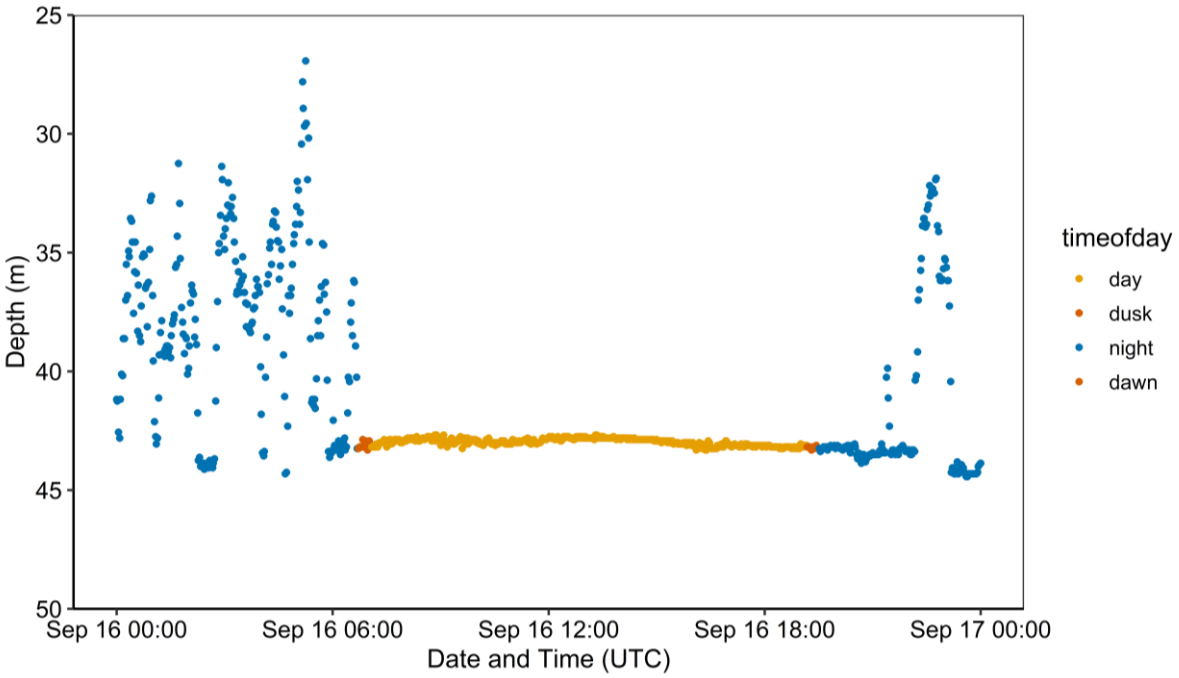

Figure 9. Observations in depth usage on the 16th of September 2021, where time of day (dawn, day, dusk and night) is denoted by different colours. Data observed from a female R. montagui 51 cm in length, tag no: A18029.

Spatial abundance using survey data

Thornback ray

IM_ST3 was selected as the best model (Table 2) to describe the spatial distribution of *R. clavata* for the stock 3a47d from 1988-2021. All three surveys (NS_BTS, FR_CGFS and NS_IBTS) and the 3 length classes were important to estimate the catch for *R. clavata*, since neither of the 95% credible intervals of the predictors of the fixed effects contained 0. The greatest catchability is found in the intercept, representing the NS_BTS survey and the unexploited immature size class (mean = -3.56, SD = 0.79; Table 3).

The best model (IM_ST3; Table 1) was then used to generate predictions of abundances on a regular grid with 5km2 cells, for each year and for three size classes. The grid was bounded by the mesh boundary used for fitting the model. 1000 abundance simulations were generated for each grid cell, year, and size class from the approximated posterior of the fitted model. At each grid location, point sampling of bathymetry determined depth. Locations in the SPDE are estimated to be correlated (≥0.1) up to a range of 120km (Figure 11).

The survey with the highest catchability (NS-BTS; Table 3) was chosen for predictions. For the predictions the swept area was equivalent to surface Area of the prediction grid cells to obtain expected count in each of the prediction grid cells. Size class specific catchability was accounted for by multiplying the expected counts with the gear efficiency of the average length per size class, based on gear efficiencies for *R. clavata* obtained from Walker et al. (2017).

The trend for Year, modelled as a iid random effect, was estimated to follow a significant positive trend since 2008 (Figure 10). The trends for Depth differ for the 3 size class categories indicate that there is a significant negative depth trend for both exploited size classes at low depth ranges (Figure 10).

A weight-length equation was applied to estimate mean weight per size class:

$$W = aL^w$$

where *W* is the mean weight per size class in grams, *L* is the average Length of the maturity size class in cm. *a* and *b* parameters were obtained sex for the North Sea ecoregion from McCully et al. (2012) by averaging across. Biomass estimates per grid cell and size class were obtained by multiplying the catchability adjusted predicted counts with the estimated mean weight per size class.

Posterior estimates of the spatial random effect indicate intrinsic spatio-temporal variability of the species distribution not captured by other covariates in the model (Figure 12). The estimated spatial random effects for *R. clavata* can clearly change over the period from 1988 to 2021 (e.g. see increase in spatial abundance in the German Bight since 2013 that appears to be a result of an expansion of the population from the English Channel).

Table 2. INLA model evaluation results for thornback ray (Raja clavata): Summary of model's deviance information criterion (DIC), and the Watanabe–Akaike information criterion (WAIC). The best model, as indicated by DIC and WAIC is indicated in bold.

Type	Model ID	Fixed Effects	Random Effects	DIC	WAIC
non-spatial					
	IM_NS2	Exploit_Maturity + SurveyQuarter + logSweptAreakm2	Year_iid	69,231	69,363
	IM_NS3	Exploit_Maturity + SurveyQuarter + logSweptAreakm2	Year_iid + Depth_Unexploited_Immature RW1 + Depth_Exploited_Immature RW1 + Depth_Expoited_Mature RW1	66,396	66,667
	IM_NS4	Exploit_Maturity + SurveyQuarter + logSweptAreakm2 + EUNIS2019D substrate	Year_iid + Depth_Unexploited_Immature RW1 + Depth_Exploited_Immature RW1 + Depth_Expoited_Mature RW1	64,558	64,862
	IM_NS5	Exploit_Maturity + SurveyQuarter + logSweptAreakm2 + EUNIS2019C	Year_iid + Depth_Unexploited_Immature RW1 + Depth_Exploited_Immature RW1 + Depth_Expoited_Mature RW1	64,136	64,460
	IM_NS6	Exploit_Maturity + SurveyQuarter + logSweptAreakm2 + Substrate	Year_iid + Depth_Unexploited_Immature RW1 + Depth_Exploited_Immature RW1 + Depth_Expoited_Mature RW1	64,477	64,778
spatial					
	IM_S2	Exploit_Maturity + SurveyQuarter + logSweptAreakm2	Year_iid	55,234	55,418
	IM_S3	Exploit_Maturity + SurveyQuarter + logSweptAreakm2	Year_iid + Depth_Unexploited_Immature RW1 + Depth_Exploited_Immature RW1 + Depth_Expoited_Mature RW1	54,345	54,561
	IM_S4	Exploit_Maturity + SurveyQuarter + logSweptAreakm2 + EUNIS2019D substrate	Year_iid + Depth_Unexploited_Immature RW1 + Depth_Exploited_Immature RW1 + Depth_Expoited_Mature RW1	54,349	54,569
	IM_S5	Exploit_Maturity + SurveyQuarter + logSweptAreakm2 + EUNIS2019C	Year_iid + Depth_Unexploited_Immature RW1 + Depth_Exploited_Immature RW1 + Depth_Expoited_Mature RW1	54,374	54,572
	IM_S6	Exploit_Maturity + SurveyQuarter + logSweptAreakm2 + Substrate	Year_iid + Depth_Unexploited_Immature RW1 + Depth_Exploited_Immature RW1 + Depth_Expoited_Mature RW1	54,332	54,555
spatio-temporal					
	IM_ST2	Exploit_Maturity + Survey + logSweptAreakm2	Year_iid	53,570	53,556
	IM_ST3	**Exploit_Maturity + Survey + logSweptAreakm2**	**Year_iid + Depth_Unexploited_Immature RW1 + Depth_Exploited_Immature RW1 + Depth_Expoited_Mature RW1**	**52,828**	**52,731**

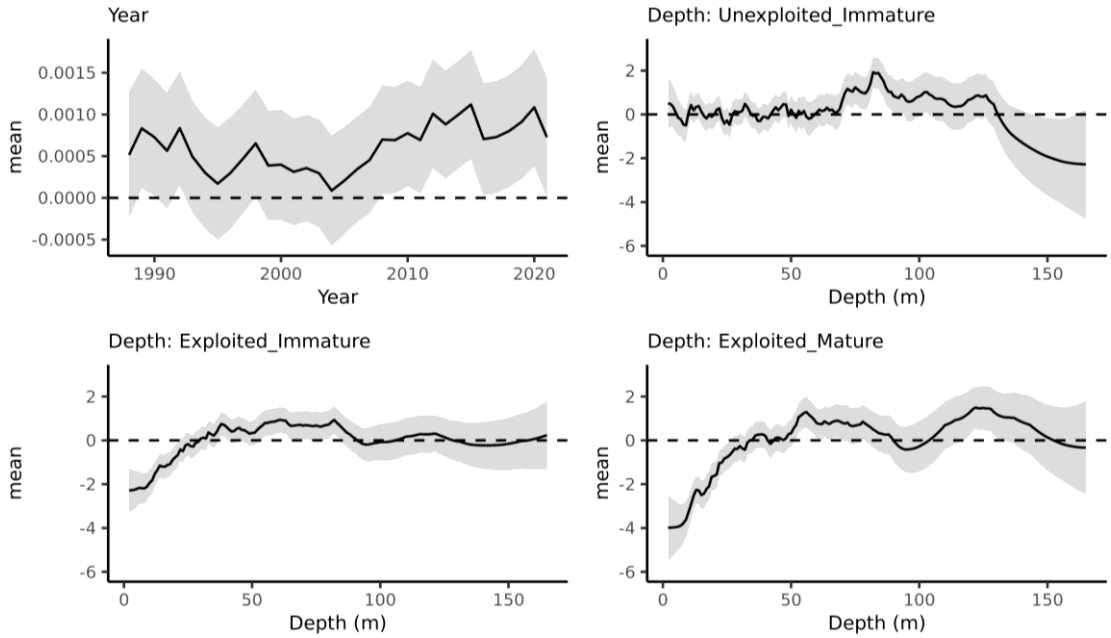

Figure 10. Trends of estimated random effect of Year (iid) and Depth (random walk) for 3 size classes with 95% credible intervals.

Table 3. Summary of the marginal posterior distribution of the fixed effects, hyperparameters for the best INLA model IM_ST3 for Raja clavata. For each parameter the mean, standard deviation, and 95% (Q0.025-Q0.975) credible intervals are provided.

Group	Parameter	Mean	SD	Q0.025	Q0.975	Description
Predictors						
	Intercept (NS-BTS, Unexpl_Immat)	-3.56	0.79	-5.10	-2.02	
	Exploit_Maturity: Exploited_Mature	-1.54	0.22	-1.98	-1.10	
	Survey: NS-IBTS	-1.11	0.06	-1.22	-0.99	
	Survey: FR-CGFS	-0.59	0.07	-0.72	-0.46	
Hyper-parameters						
	k	0.22	0.00	0.21	0.23	Size for nbinomial observations
	ρ_{η_t}	$3.38^{E}5$	$1.95^{E}4$	$3.02^{E}5$	$3.79^{E}5$	Precision for Year
	$\rho_{\eta_{d,\ m=0}}$	0.41	0.02	0.38	0.46	Precision for Depth: Unexploited_ Immature
	$\rho_{\eta_{d,\ m=1}}$	1.14	0.06	1.01	1.26	Precision for Depth: Exploited_ Immature
	$\rho_{\eta_{d,\ m=2}}$	0.54	0.03	0.48	0.60	Precision for Depth: Exploited_Mature
	θ_1	1.33	0.04	1.25	1.41	Mean of $\nu_{i,t}$
	θ_2	-3.74	0.04	-3.82	-3.66	SD of $\upsilon_{i,t}$
Spatio-temporal parameters						
	ρ_t	0.86	0.01	0.84	0.87	Temporal correlation between consecutive time steps for $\upsilon_{i,t}$
	K	0.02	0.00	0.02	0.03	
	σ_υ	10.00	0.75	8.73	11.66	

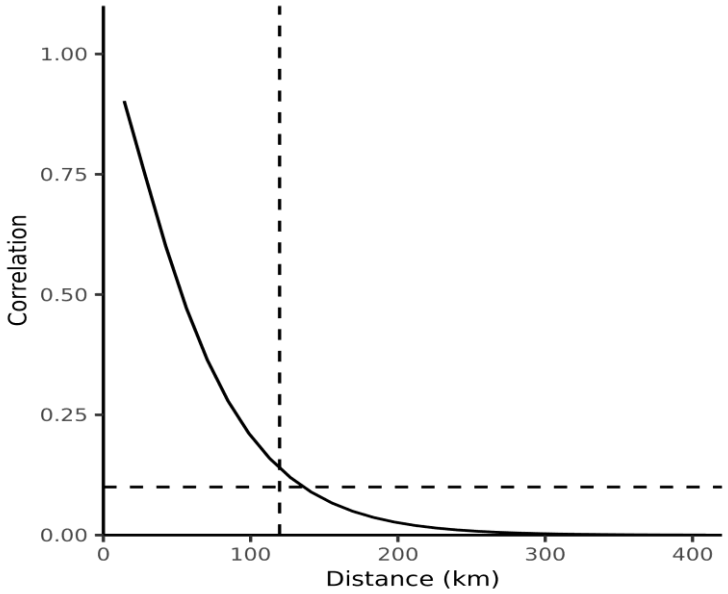

Figure 11. Matérn correlation function (solid line) describes the correlation of locations in the SPDE model in relation to their distance to each other. The vertical dashed line indicates the estimated range (120 km), at which the correlation is approximately 0.1 (horizontal dashed line).

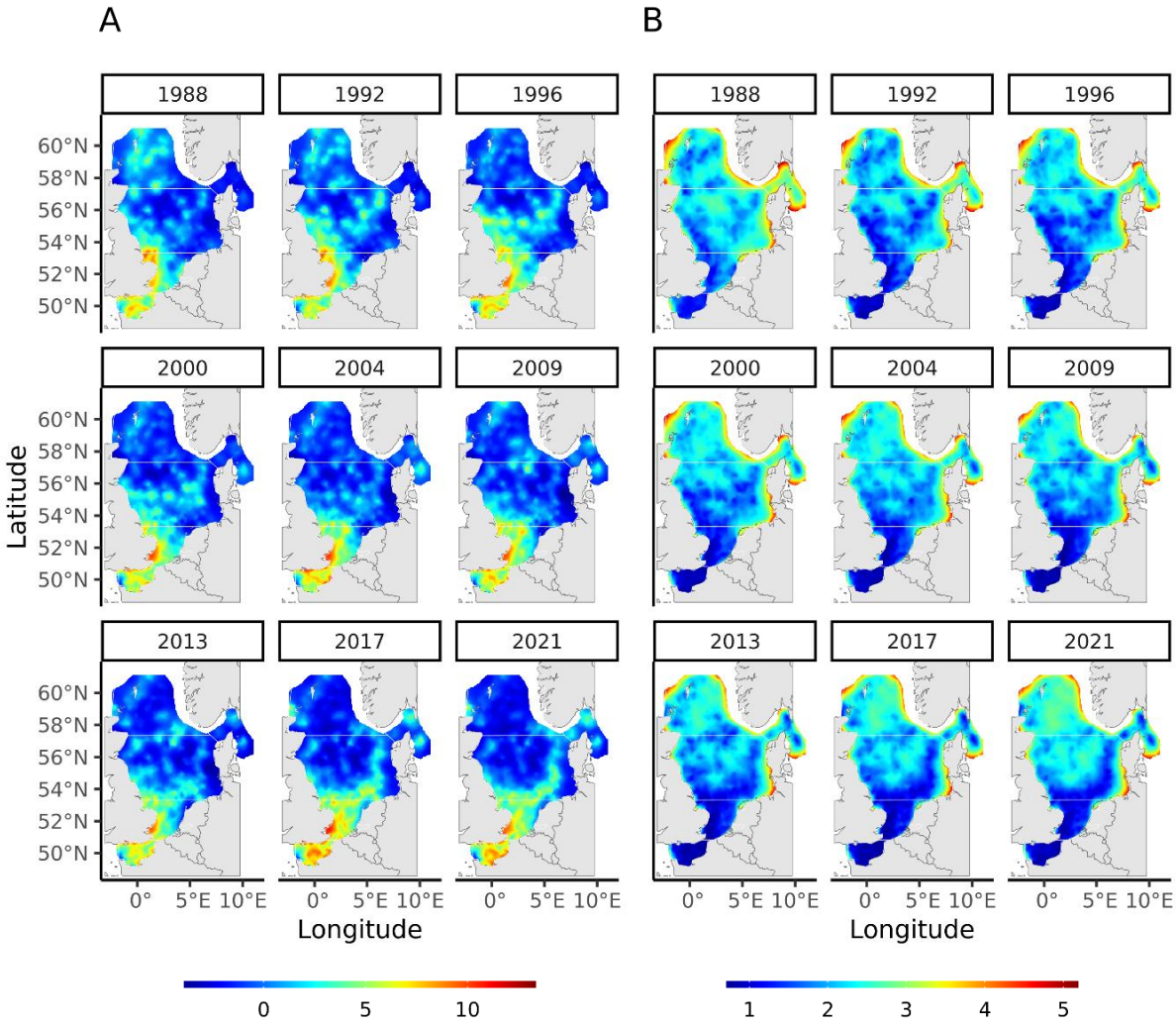

Figure 12. Posterior mean (A) and SD (B) of the spatial random effect by 5km2 from 1988 to 2021 for every 4 years.

Blonde ray

Spatio-temporal model 2 was identified as the best model for *R. brachyura,* as it had the lower DIC (7097.5) and WAIC (6940.7) which suggests better performance (Table 4). There was a marked increase observed of the exploited mature size class (of individuals > 81 cm) (Figure 13). The extent of the spatial correlation in the data was slightly smaller than for *R. clavata*, being 100 km (Figure 14). This suggest a slightly more "patchy" distribution of *R. brachyura* compared to *R. clavata*. The estimated spatial random effects for *R. brachyura* over the period from 1988 to 2021 indicate the spatio-temporal variation in the distribution of the species (Figure 15). The figure represents how much spatial location affects abundance estimates and visualises the estimated spatial effect on abundance. From 1988, an increasingly pronounced hotspot of spatial random effect can be observed in division 4c, 7d and 4a. Another increasingly pronounced hotspot of spatial random effect can be observed extending from division 4c to 4b and seem to be also originating in 4c.

Table 4. INLA model evaluation results for blonde ray (R. brachyura): Summary of model's deviance information criterion (DIC), and the Watanabe–Akaike information criterion (WAIC). The best model as estimated by DIC and WAIC is in bold.

Type	Model ID	Fixed Effects	Random Effects	DIC	WAIC
non-spatial					
	IM_NS2	Exploit_Maturity+ SurveyQuarter + logSweptAreakm2	Year_Unexploited_Immature RW1 + Year_Exploited_Immature RW1 + Year_Exploited_Mature RW1	9,321	9,357
	IM_NS3	Exploit_Maturity+ SurveyQuarter + logSweptAreakm2	Year_Unexploited_ImmatureRW1 + Year_Exploited_Immature RW1 + Year_Exploited_Mature RW1 + Depth_Immature RW1 + Depth_Mature RW1	8,987	9,031
	IM_NS4	Exploit_Maturity+ SurveyQuarter + logSweptAreakm2 + EUNIS2019D substrate	Year_Unexploited_ImmatureRW1 + Year_Exploited_Immature RW1 + Year_Exploited_Mature RW1 + Depth_Immature RW1 + Depth_Mature RW1	8,564	8,597
	IM_NS5	Exploit_Maturity+ SurveyQuarter + logSweptAreakm2 + EUNIS2019C	Year_Unexploited_ImmatureRW1 + Year_Exploited_Immature RW1 + Year_Exploited_Mature RW1 + Depth_Immature RW1 + Depth_Mature RW1	8,493	8,510
	IM_NS6	Exploit_Maturity+ SurveyQuarter + logSweptAreakm2 + Substrate	Year_Unexploited_ImmatureRW1 + Year_Exploited_Immature RW1 + Year_Exploited_Mature RW1 + Depth_Immature RW1 + Depth_Mature RW1	8,635	8,652
spatial					
	IM_S2	Exploit_Maturity+ SurveyQuarter + logSweptAreakm2	Year_Unexploited_ImmatureRW1 + Year_Exploited_Immature RW1 + Year_Exploited_Mature RW1	7,171.6	7,109.3
	IM_S3	Exploit_Maturity+ SurveyQuarter + logSweptAreakm2	Year_Unexploited_ImmatureRW1 + Year_Exploited_Immature RW1 + Year_Exploited_Mature RW1 + Depth_Immature RW1 + Depth_Mature RW1	7,250.8	7,187.3
	IM_S4	Exploit_Maturity+ SurveyQuarter + logSweptAreakm2 + EUNIS2019D substrate	Year_Unexploited_ImmatureRW1 + Year_Exploited_Immature RW1 + Year_Exploited_Mature RW1 + Depth_Immature RW1 + Depth_Mature RW1	7,248.8	7,188.7
	IM_S5	Exploit_Maturity+ SurveyQuarter + logSweptAreakm2 + EUNIS2019C	Year_Unexploited_ImmatureRW1 + Year_Exploited_Immature RW1 + Year_Exploited_Mature RW1 + Depth_Immature RW1 + Depth_Mature RW1	7,263.2	7,201.8
	IM_S6	Exploit_Maturity+ SurveyQuarter + logSweptAreakm2 + Substrate	Year_Unexploited_ImmatureRW1 + Year_Exploited_Immature RW1 + Year_Exploited_Mature RW1 + Depth_Immature RW1 + Depth_Mature RW1	7,356.8	7,266.3
spatio-temporal					
	IM_ST2	Exploit_Maturity+ Survey + logSweptAreakm2	Year_Unexploited_Immature RW1 + Year_Exploited_Immature RW1 + Year_Exploited_Mature RW1	7,103.3	6,952.7
	IM_ST2_pred	**Exploit_Maturity+ Survey + logSweptAreakm2**	**Year_Unexploited_Immature RW1 + Year_Exploited_Immature RW1 + Year_Exploited_Mature RW1**	**7,097.5**	6,940.7

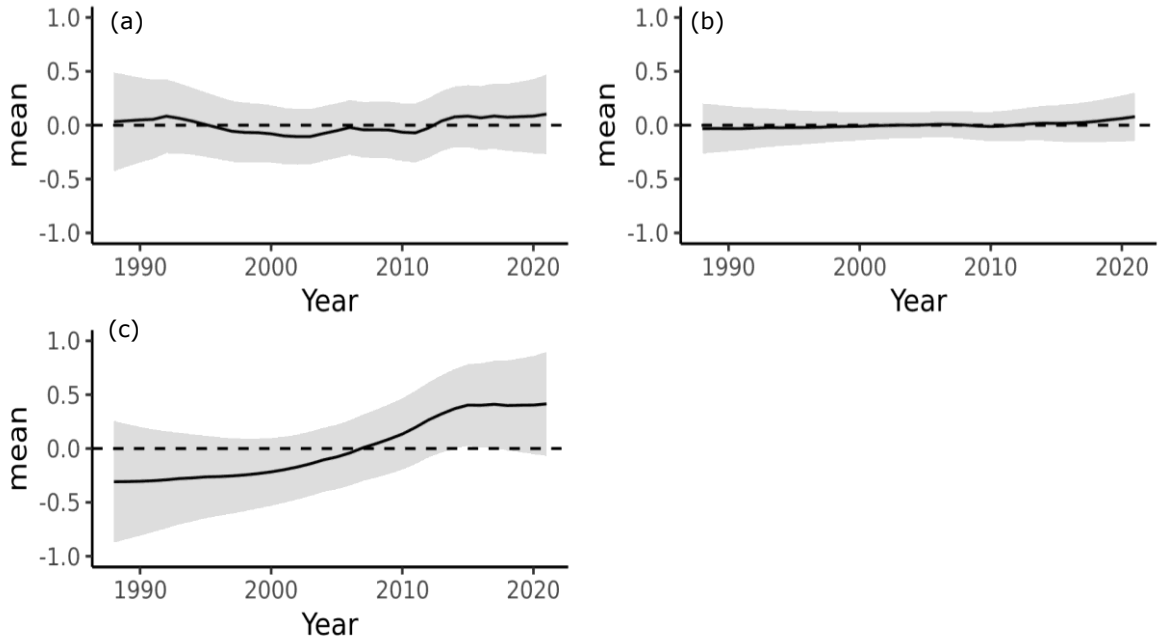

Figure 13. Trends of estimated random effect of Year for 3 size classes with 95% credible intervals: (a) unexploited immatures (<50cm) (b) exploited immatures (>= 50cm & < 71cm), (c) exploited matures (>= 71cm).

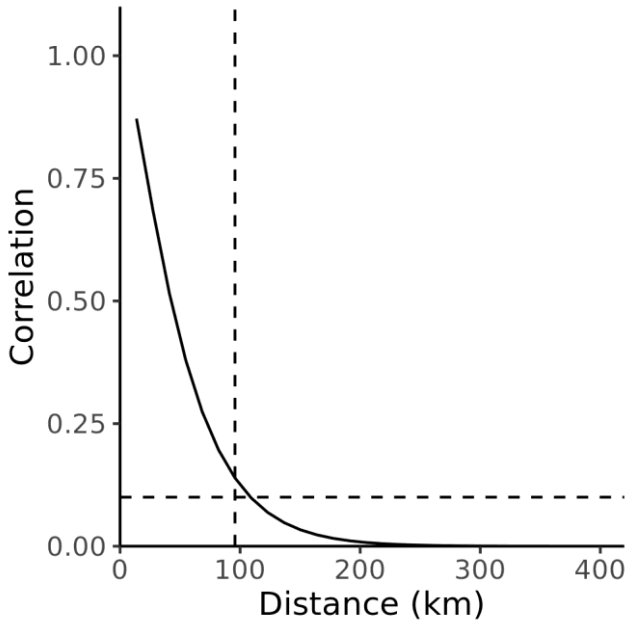

Figure 14. Matérn correlation function (solid line) describes the correlation of locations in the SPDE model in relation to their distance to each other. The vertical dashed line indicates the estimated range (100 km), at which the correlation is approximately 0.1 (horizontal dashed line).

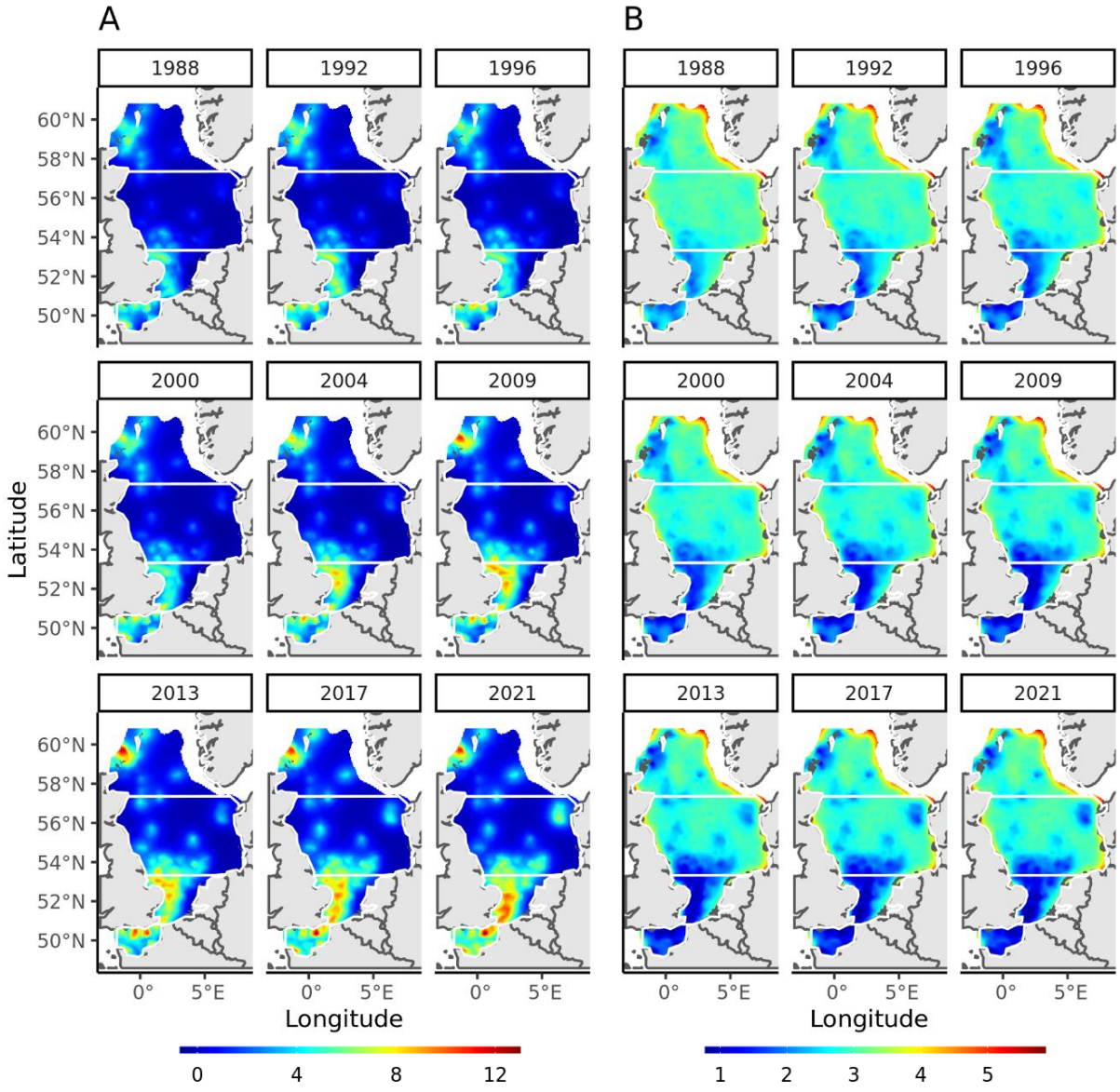

Figure 15. Posterior mean (A) and standard deviation (B) of the spatial random effect by 5km2 from 1988 to 2021 for every 4 years. Note that these effects are on a log scale.

Population genetic structure

Thornback ray

Genotypes for a total of 7214 unique *Raja clavata* samples were available (Table 5 & Figure 16). These were collected through a variety of projects, including the "bridging knowledge gaps" project. After quality control, 5048 samples remained with 4797 loci for genetic population structure analyses (Table 6).

Table 5. Initial and Postfiltering counts of Raja clavata by Ecoregion and sex.

		Sample size		Sex	
Ecoregion	**Year**	**Initial**	**Post-filtering**	**No. of males**	**No. of females**
Celtic Seas	2003-2004	298	132	66	66
Greater North Sea	2003-2022	2,957	2,032	967	1,065
Greater North Sea (unkown location)	2018-2022	205	94	22	72
Bay of Biscay & Iberian Coast	2011-2020	3,754	2,790	1,358	1,432
Total	2003-2022	7,214	5,048	2,413	2,635

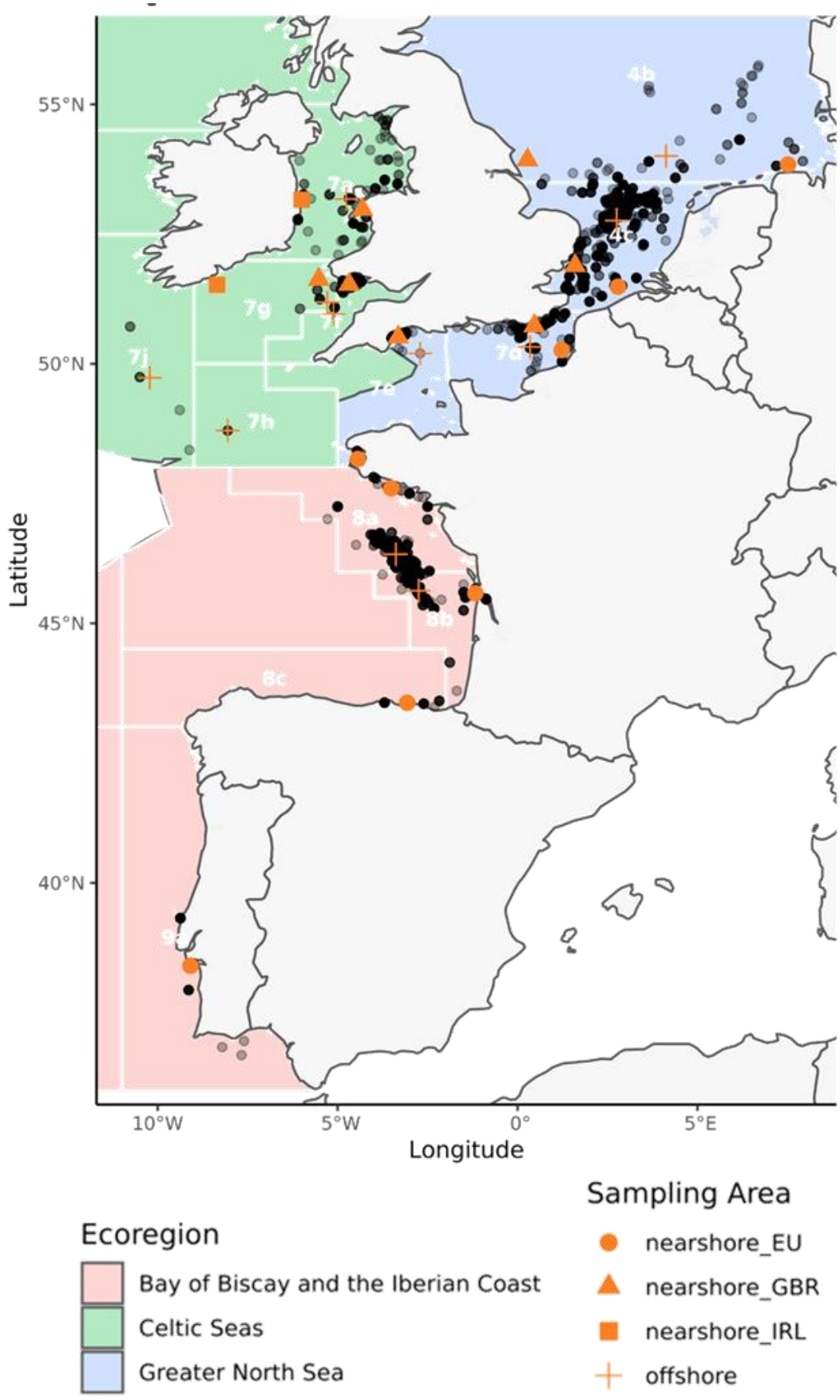

Figure 16. Spatial locations of 7214 Raja clavata samples (black points) collected and genotyped. Orange symbols indicate the average location for samples collected in sampling areas (based on ICES divisions and distance to shore).

Table 6. Summary of filtering steps for Raja clavata.

Filtering Step	No. samples remaining	No. loci remaining
No cleanup	7,407	9,120
Remove misidentified & duplicated samples, GC filter, remove non-scoring loci, and monomorphic loci	7,214	7,027
Sample call rate filter: ≥0.98	5,058	5,958
Loci call rate filter: ≥0.95	5,058	5,800
Filter loci for minor allele frequency: ≥0.05	5,058	5,753
Remove unintentional replicates	5,056	5,753
Remove sex-linked loci	5,056	5,730
Remove secondary loci	5,056	4,991
Remove one loci of each loci pair in Linkage disequilibrium: >0.1	5,056	4,797
Remove one individual of each individual identified as first or second order kin pair	5,048	4,797

The DAPC with ICES divisions used as a grouping prior for samples indicates both large (across Ecoregions) and small scale (within Ecoregions) spatial population structure. On A large spatial scale, samples are clearly clustered by Ecoregions (colour of subarea labels). The Celtic sea samples cluster slightly separately from the Greater North Sea samples, whereas the Bay of Biscay samples clearly cluster separately to the Celtic sea and the Greater North Sea samples. An exception to this are samples from the 7e_nearshore_EU sample area from the Greater North Sea Ecoregion that cluster with samples from the 8a_nearshore_EU area from the Bay of Biscay and Iberian Coast Ecoregion (Figure 17), indicating an exception to the otherwise little population structure observed within the Greater North Sea Ecoregion. This appears reasonable as these two locations are geographically very close to each other. Within the Celtic Seas little mall scale population structure appears to be indicated by clustering 7j_offshore, 7h_offshore, and 7f_offshore separate to the remaining areas in the Celtic Seas (Figure 17). Small scale genetic population structure appears to be most distinct within the Bay of Biscay and Iberian coast ecoregion. 8a_offshore and 8b_offshore samples cluster closely together, while 8a_nearshore_EU, 8b_nearshore_EU, 8c_nearshore_EU, and 9a_nearshore_EU samples cluster away from the respective offshore samples. This indicates genetic population structure within the Bay of Biscay between offshore and nearshore samples and provides additional evidence for distinct local populations of thornback ray in the bay of Biscay, as indicated by finding no evidence of demographic connectivity in a previous study (Trenkel et al. 2022).

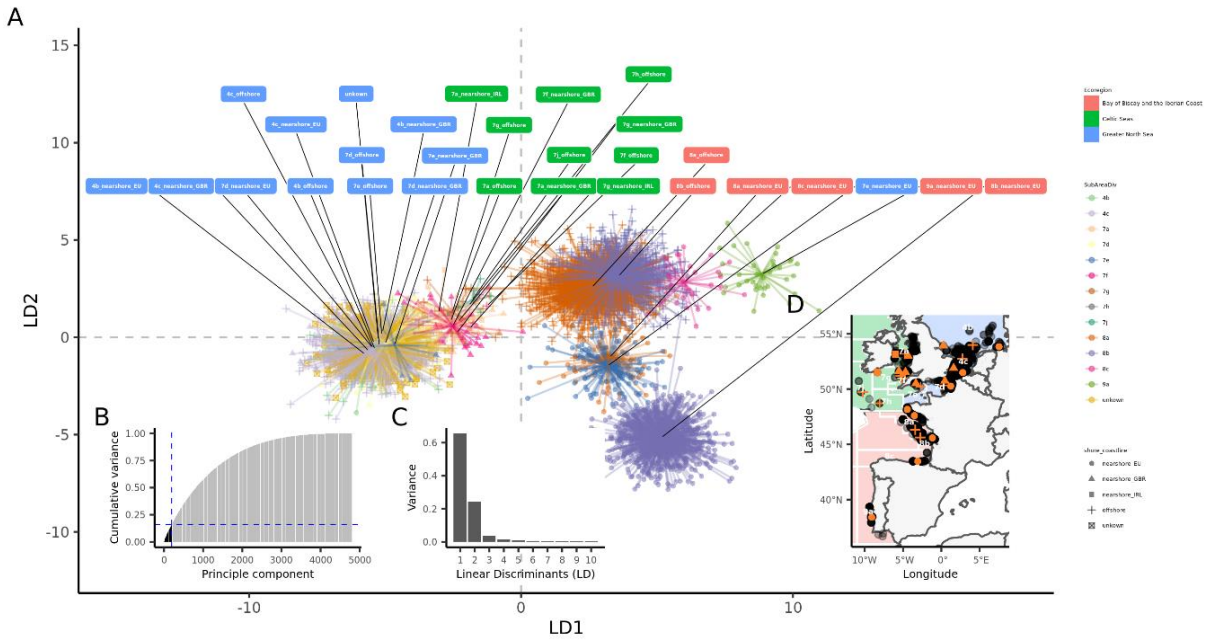

Figure 17. Discriminant analysis of principal components with grouping Prior based on ICES divisions(A). (B) Cumulative variance of optimal number of 83 PCs retained for DAPC. (C) Variance of linear discriminants retained in DAPC. (D) Sample locations.

The best DAPC model without prior grouping was the model with 3 clusters (K) as indicated by the lowest BIC (Figure 18) and the "elbow" in the difference between BIC and slope of difference between BIC among subsequent clusters (Figure 18). The optimal number of Principal components (PCs) to retain in the DAPC was 237 (Figure 19), making up 0.19 of the cumulative variance observed (Figure 20), where the linear discriminant component 1 explained > 0.6 variance (Figure 20). The 3 proposed clusters were clearly observed in the DAPC (Figure 21Figure) and indicated the presence of large (between Ecoregion) and small (within Ecoregion) scale genetic population structure (Figure 22). The DAPC without prior differentiates on a large spatial scale samples in the Bay of Biscay and Iberian coast ecoregion from samples in the Celtic Seas and Greater North Sea ecoregion. It further indicates the presence of small scale genetic population structure within the Bay of Biscay between samples found offshore in 8a and 8b from samples found nearshore in 8a and 8b subareas. This provides additional evidence of genetically differentiable populations present in the Bay of Biscay, as seen in the DAPC with prior results as well as suggested by Trenkel et al. (2022).

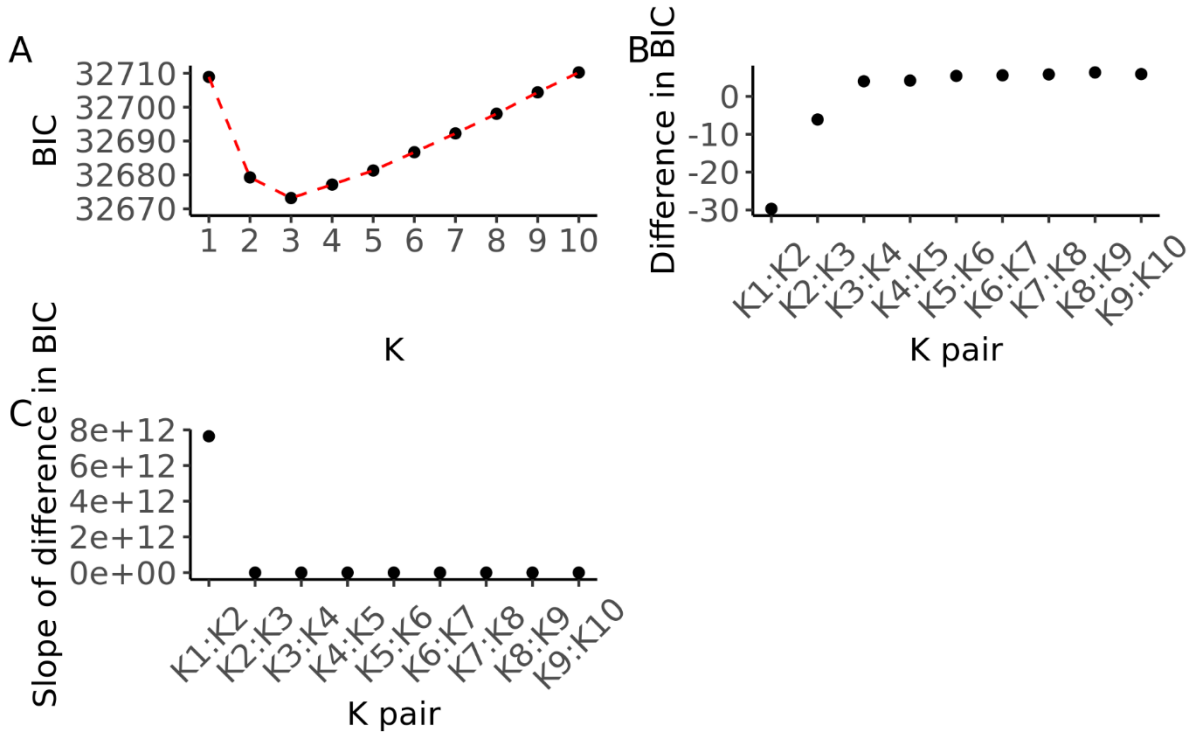

Figure 18. Cluster (K) evaluation of DAPC without prior grouping. (A) BIC for clusters, (B) Difference in BIC between clusters, and slope of difference between clusters.

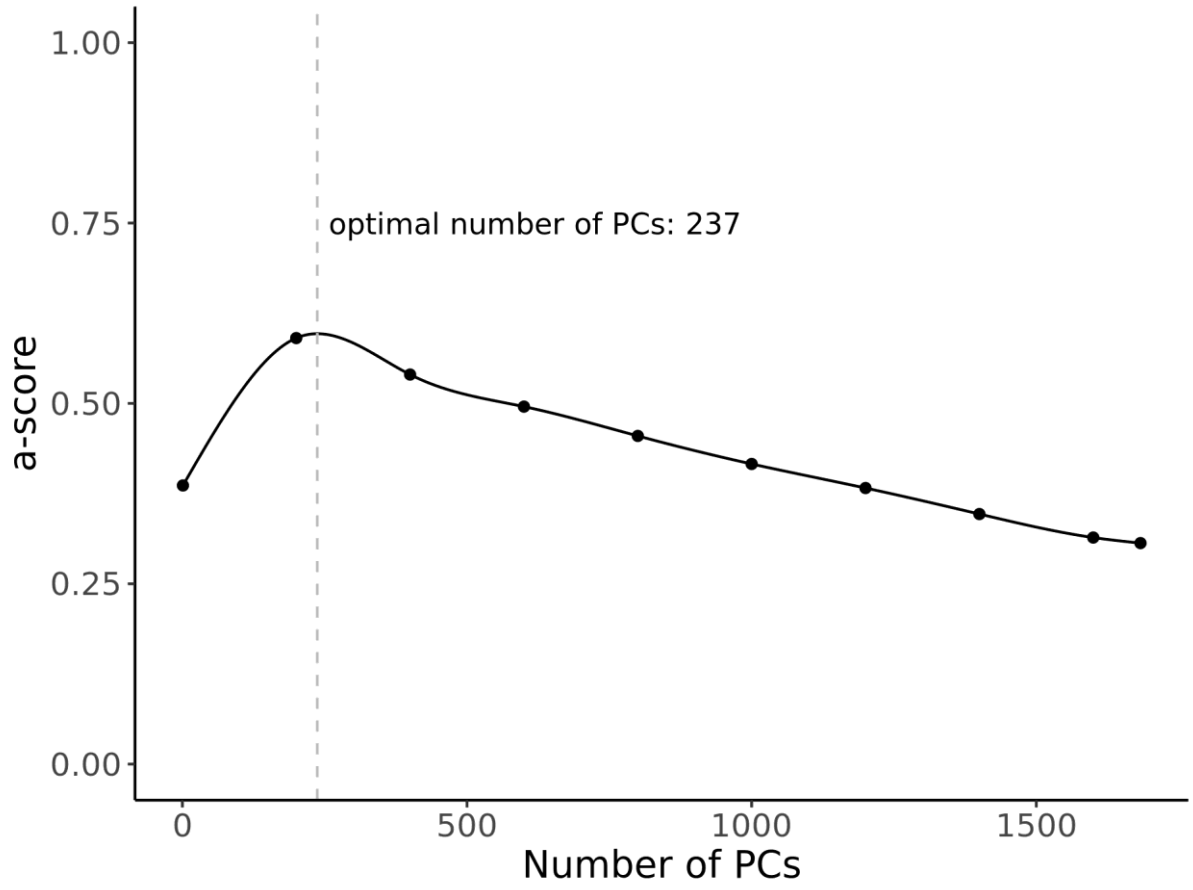

Figure 19. Estimated a-scores to determine optimal number of PCs to retain in DAPC without prior.

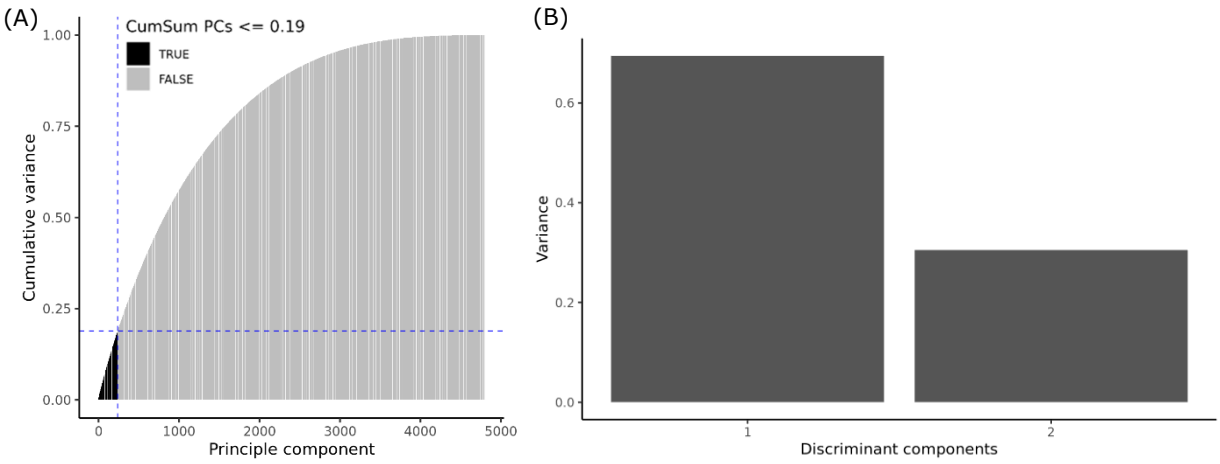

Figure 20. Cumulative variance of optimal number of 237 PCs retained for DAPC without prior (A) and variance of linear discriminants (LD) retained in DAPC without prior (B).

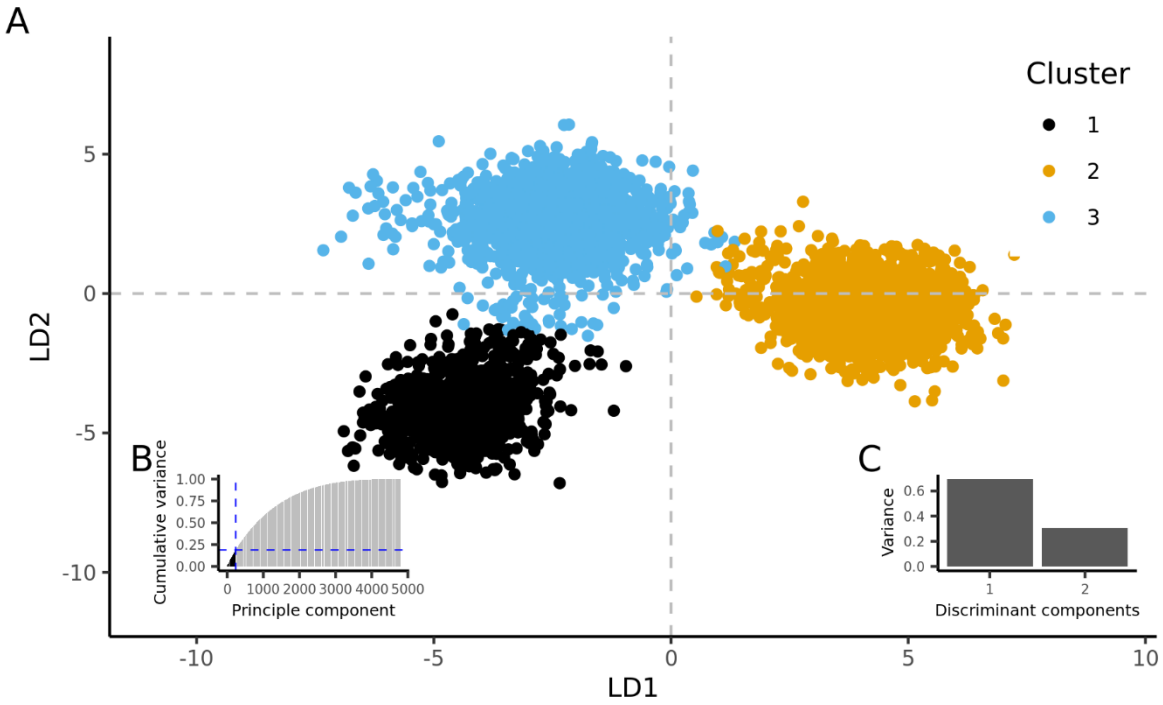

Figure 21. Discriminant analysis of principal components without grouping (A). (B) Cumulative variance of optimal number of 237 PCs retained for DAPC. (C) Variance of linear discriminants retained in DAPC.

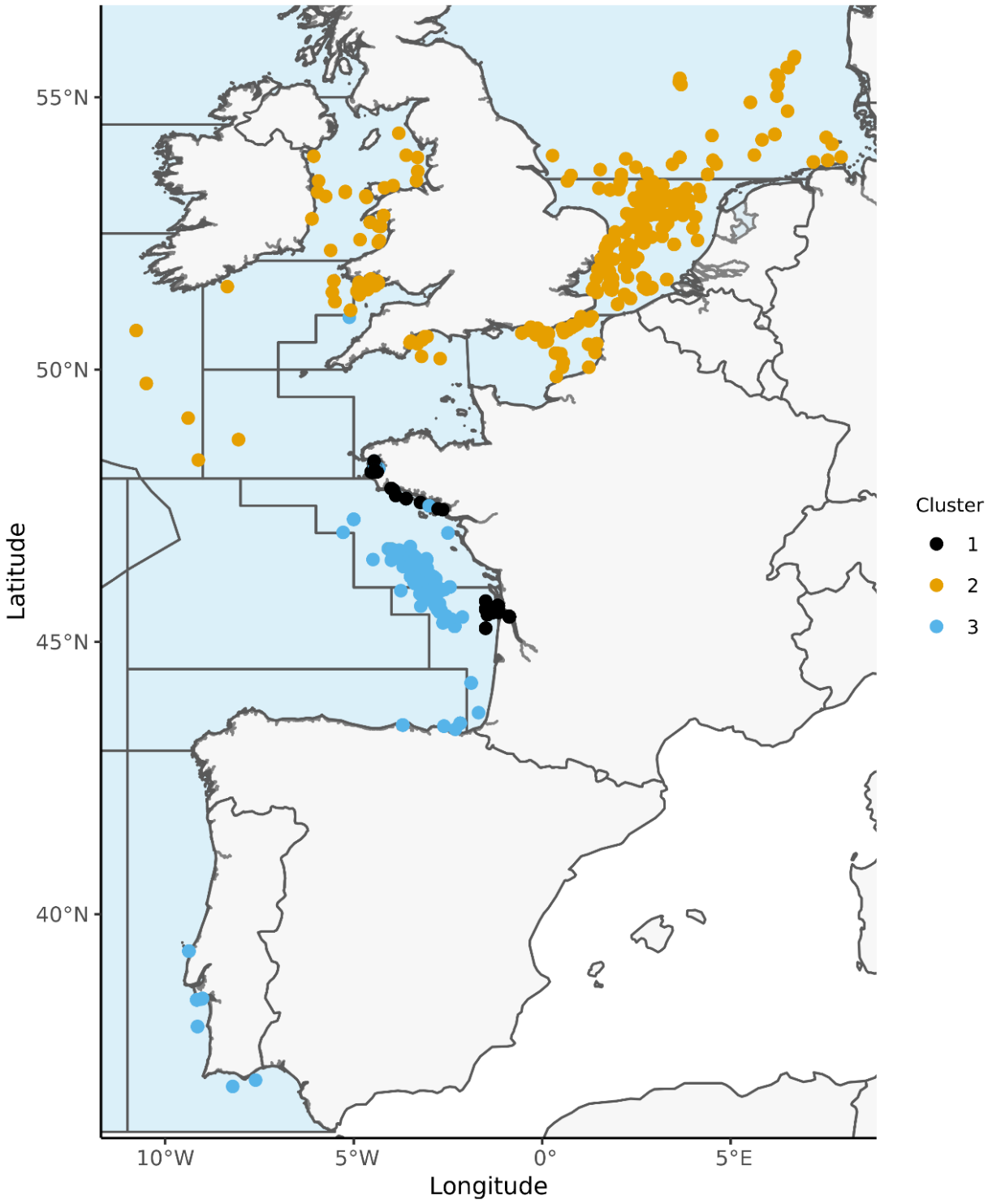

Figure 22. Raja clavata samples colour coded by cluster results of DAPC without prior.

The best admixture model with 3 clusters (K) was selected based on a low cross-entropy, the "elbow" in the difference in cross-entropy, and in the slope of difference in the cross-entropy between clusters (Figure 23Figure). Plotting the average ancestral cluster proportions by sampling area (defined as ICES division and distance to coastline) indicates the presence of large and small scale genetic population structure (Figure 24). On a large spatial scale (between Ecoregions) Celtic Sea and the Greater North Sea ecoregions can be differentiated, with cluster 3 (blue) contributing a greater proportion to the Great North Sea ecoregion, while cluster 2 (orange) appears to be more common in the Celtic Seas ecoregion (Figure). Sample areas from the Bay of Biscay and the Iberian coast can also be clearly differentiated from the Celtic

Seas and the Greater North sea ecoregion sample areas, with dominating proportion of cluster 2 (orange) and 1 (black), and reduces proportion of cluster 3 (blue) the further south samples are found (Figure). The exception, similar to DAPC with prior results, is again the sample area 8c_nearshore_EU that shows a very similar cluster proportion as the sample area 8a_nearshore_EU. On a small spatial scale, only the Bay of Biscay and Iberian coast ecoregion appears to show genetic population structure. In 8a and 8c, nearshore samples have a greater proportion of cluster 1 (black) than offshore samples, for which cluster 2 (orange) makes up the highest proportion (Figure).

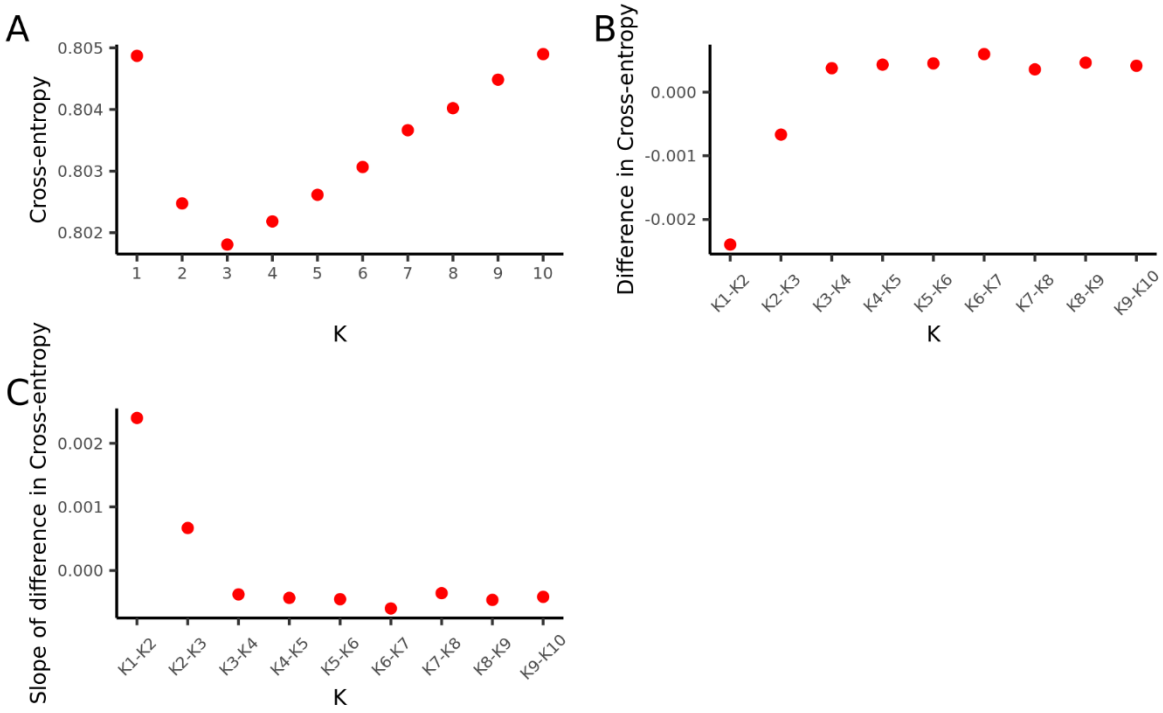

Figure 23. Cross-entropy (A), difference in Cross-entropy (B) and slope of difference in Cross-entropy (C).

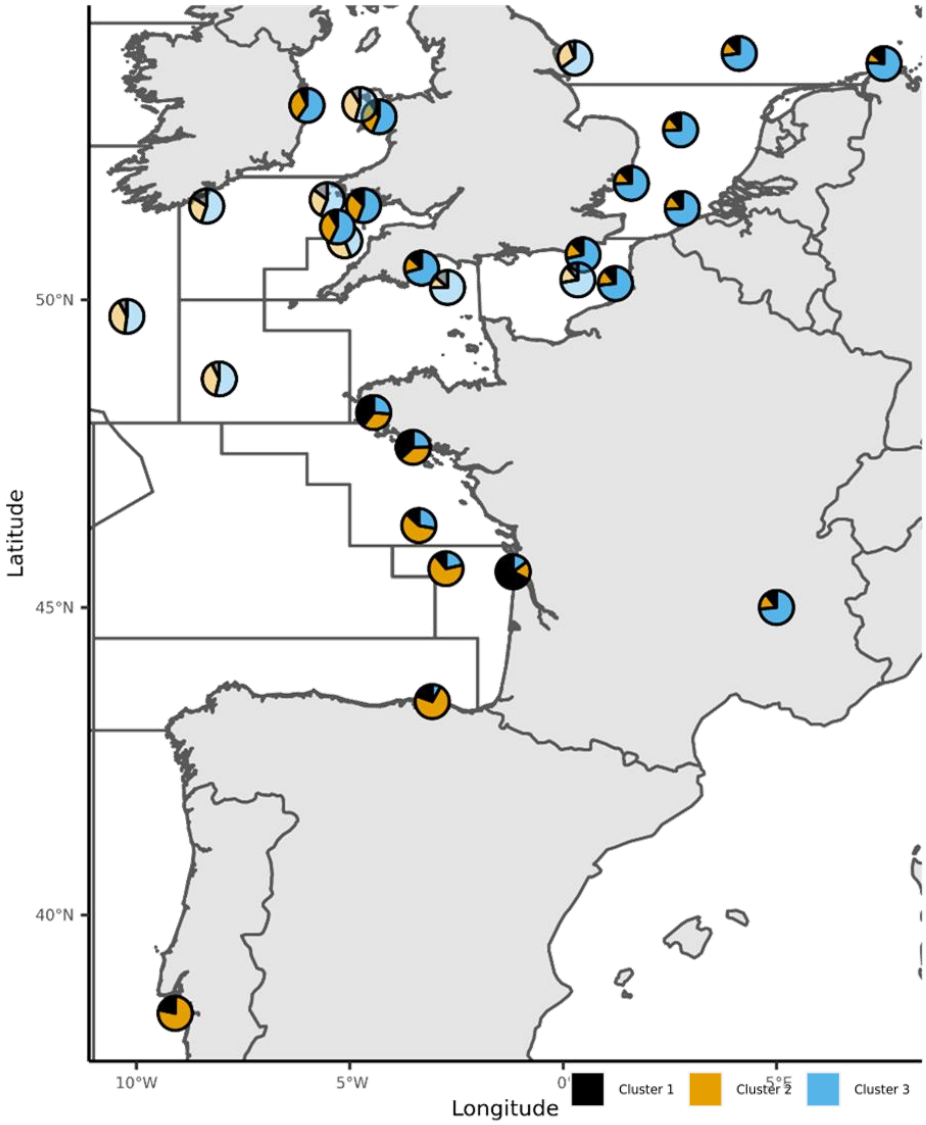

Figure 24. Average ancestry cluster proportions (admixture) grouped by sample areas (defined by ICES subareas and distance to shore) by for K=3. Transparent pie charts indicate sub-populations with sample size < 10 samples. The pie chart on France represents the combined 205 samples from the Greater North Sea ecoregions for which no spatial location could be determined.

Blonde ray

Within the Greater North Sea and the Celtic Seas a total of 934 samples of *Raja brachyura* were available, with the majority from the Greater North Sea (Table 7). After quality control, 855 samples and 2083 loci remained for genetic population structure analyses (Table 8 & Figure 25).

Table 7. Counts of Raja brachyura samples after filtering steps by Ecoregion and ICES division.

ICES ecoregion	Samples	ICES division	Samples
Celtic Seas	35	7a	19
		7f	4
		7g	12
Greater North Sea	820	4b	6
		4c	601
		7d	93
		unkown	120

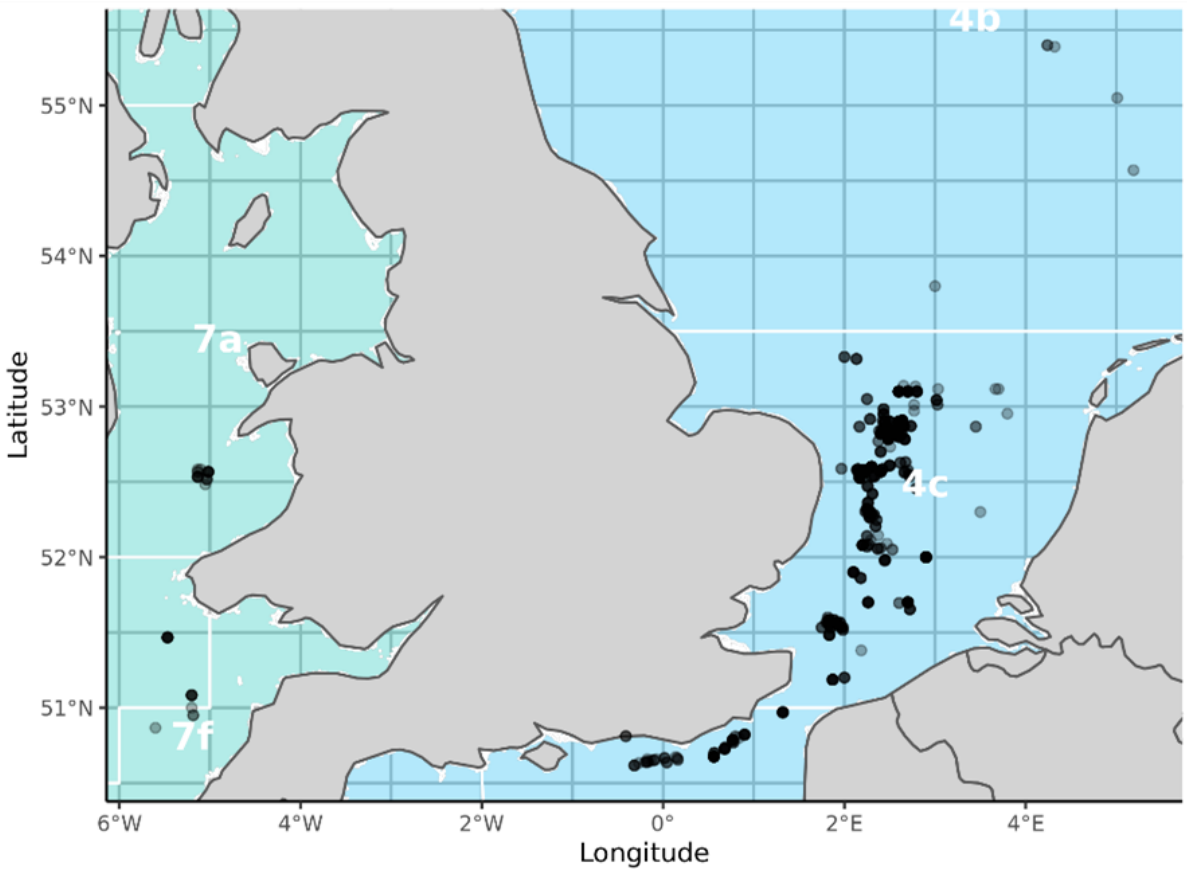

Figure 25. Spatial locations of 934 Raja brachyura samples.

Table 8. Summary of filtering steps for 934 Samples and 5925 single nucleotide polymorphism (SNP) genotyped for Raja brachyura.

Filtering Step	**No. samples remaining**	**No. loci remaining**
Removed misidentified samples, intentional duplicated samples, non-scoring loci , and monomorphic loci	934	5,925
Sample call rate filter: ≥0.85	859	5,399
Loci call rate filter: ≥0.95	859	3,376
Filter loci for minor allele frequency: ≥0.05	859	2,114
Remove unintentional replicates	855	2,114
Remove one loci of each loci pair in Linkage disequilibrium: >0.5	855	2,083

The DAPC with ICES divisions used as a grouping prior for samples clusters 7g and 7f more separated from the Greater North Sea samples, while 7a get clustered more closely to the Greater North Sea samples (Figure 26A). Within the Greater North Sea only 7d appears to cluster more separated from the other areas (Figure 26A). Samples from 4b and 4c appear to cluster together (Figure 26A), indicating a genetically similar stock. Previously, this species was split in two stocks in the North Sea, with one stock in area 4c and one stock in 4a (ICES, 2018). However, it should be noted that we have limited data available for 4b (6 samples, Table 7), and increased samples across the entire 4b area is recommended to gain a better insight into the genetic population structure.

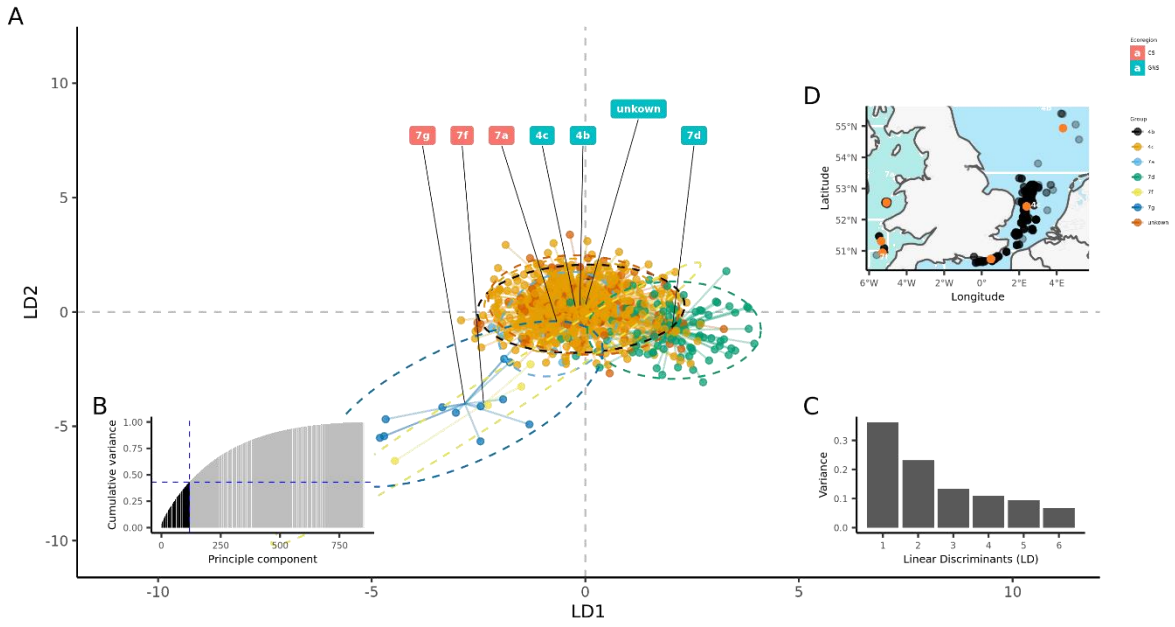

Figure 26. Discriminant analysis of principal components with grouping Prior based on ICES divisions (A). (B) Cumulative variance of optimal number of 83 PCs retained for DAPC. (C) Variance of linear discriminants retained in DAPC. (D) Sample locations.

The best DAPC model without prior grouping appears to be the model with 3 cluster (K) as indicated by the lowest BIC, and the "elbow" in the difference and slope of difference between subsequent clusters (Figure 27). The optimal number of Principal components (PCs) to retain in the DAPC is 83 (Figure 28), which make up 0.34 of the cumulative variance observed (Figure 29). A differentiation in the proposed 3 clusters can observed in the DAPC (Figure 29), however no apparent clustering by spatial sampling locations across Ecoregion (Celtic Sea or Greater North Sea Samples) or ICES division is suggested by this model (Figure 30). The individuals sampled in 4b get clustered into cluster 1 that also includes samples collected in the Greater North Sea and Celtic Sea (Figure 31). Further investigation is required how quality control and filtering steps changes the clustering results. A lack of samples in 4b also make it difficult for now to draw reliable conclusions.

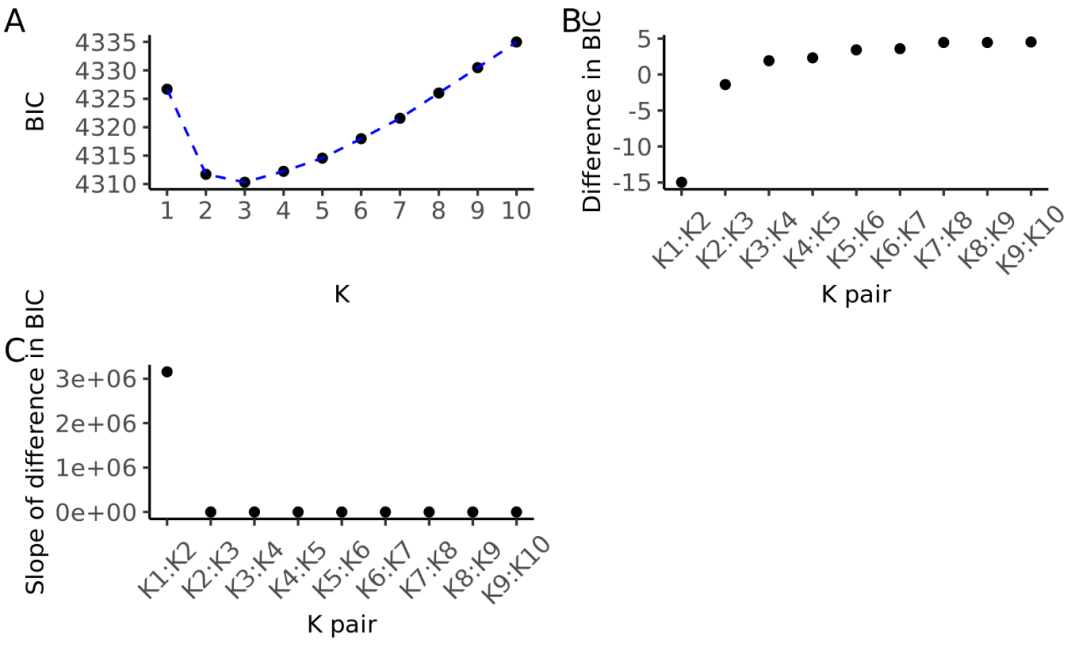

Figure 27. Cluster (K) evaluation of DAPC without prior grouping. (A) BIC for clusters, (B) Difference in BIC between clusters, and slope of difference between clusters.

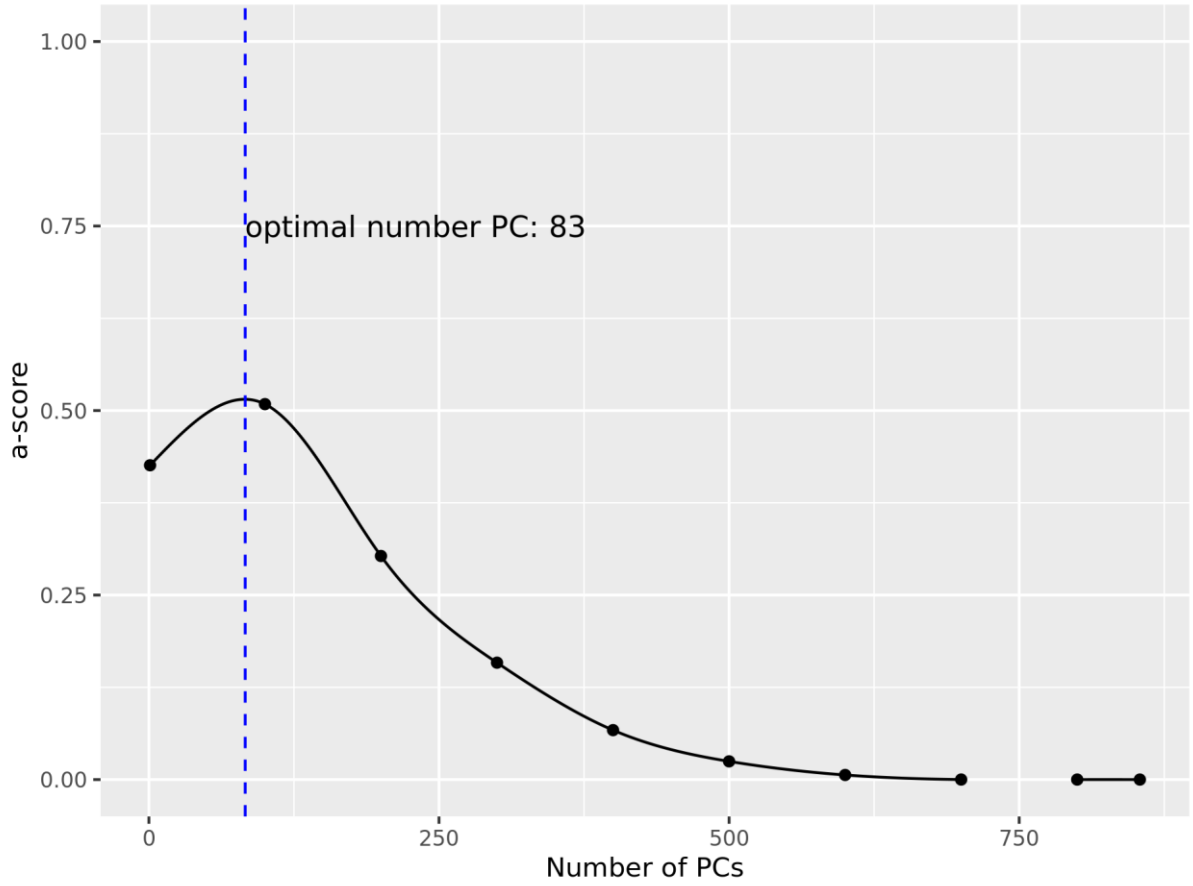

Figure 28. Estimated a-scores to determine optimal number of PCs to retain in DAPC without prior.

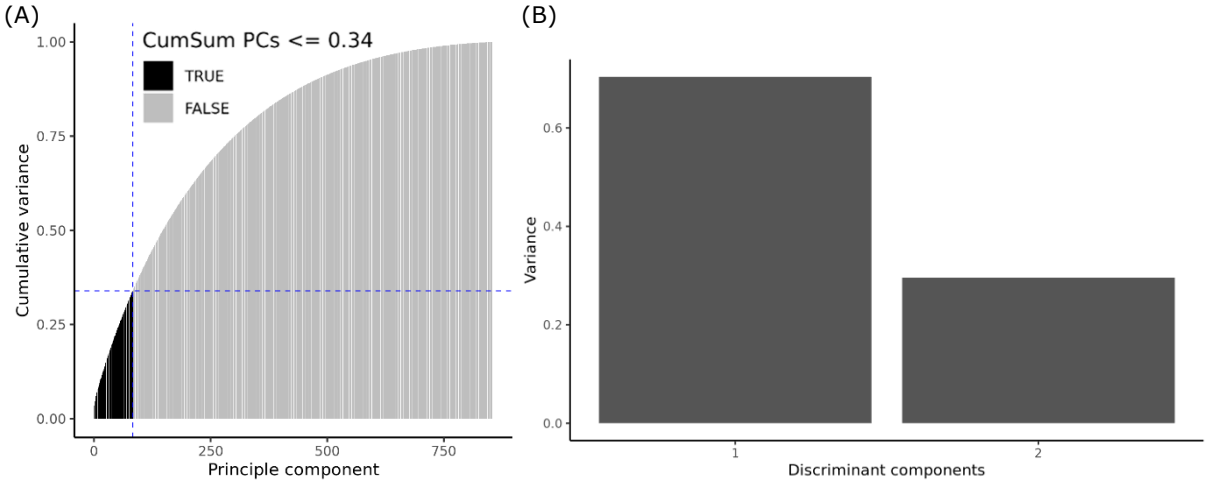

Figure 29. Cumulative variance of optimal number of 83 PCs retained for DAPC without prior.

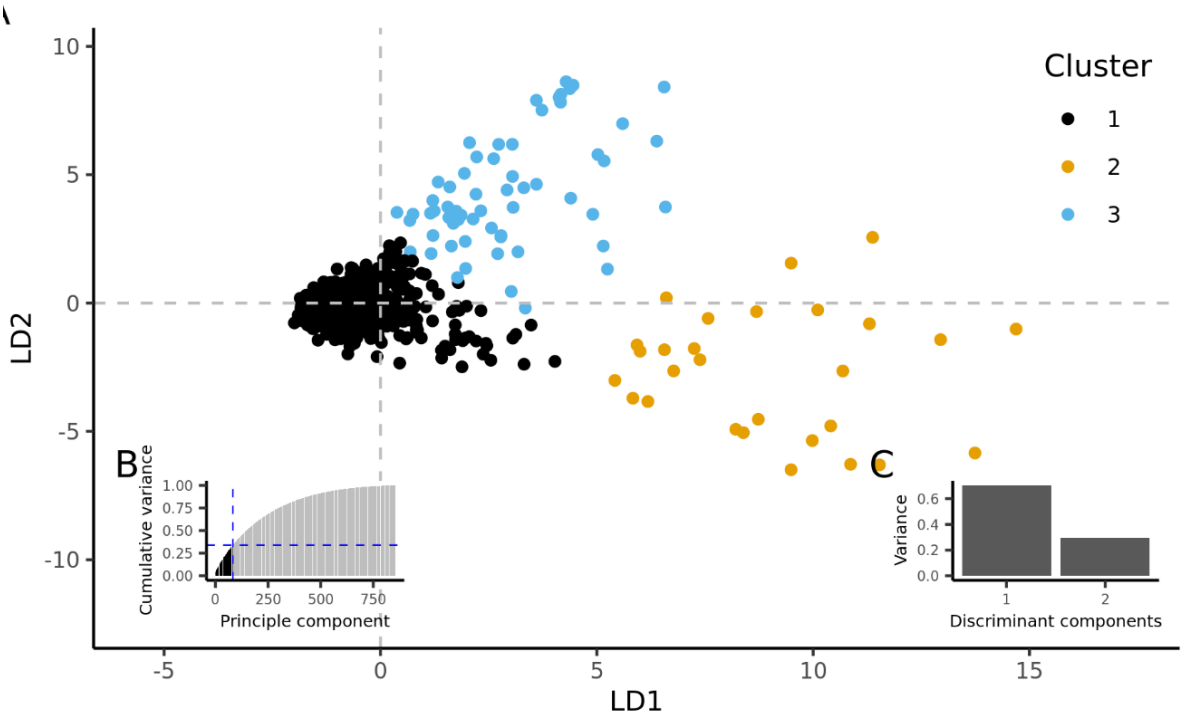

Figure 30. DAPC without prior for Raja brachyura (A) with 3 clusters (A), cumulative variance of optimal 83 PCs (B), and Variance of Linear Discriminants in the DAPC (C).

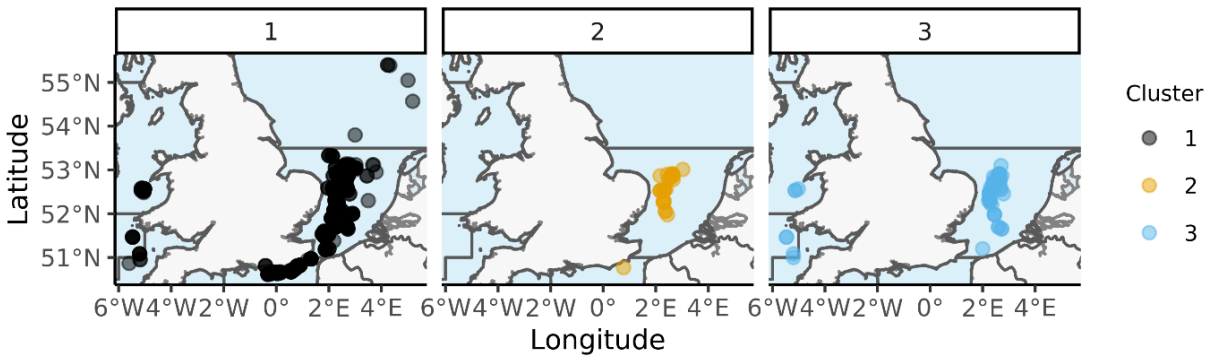

Figure 31. Sample locations of Raja brachyura samples colour coded by cluster results of DAPC without prior.

The best admixture model with 3 clusters (K) is selected based on a low cross-entropy, the "elbow" in the difference in cross-entropy and in the slope of difference in the cross-entropy (Figure 32) between clusters. Plotting the average ancestral cluster proportions by division indicates some population structure between the Celtic Sea and the Greater North Sea ecoregion, with cluster 3 (blue) contributing a greater proportion

to the Celtic Sea samples. Some minor population structure appears to be present within both within Celtic Sea and the Greater North Sea (Figure 33).

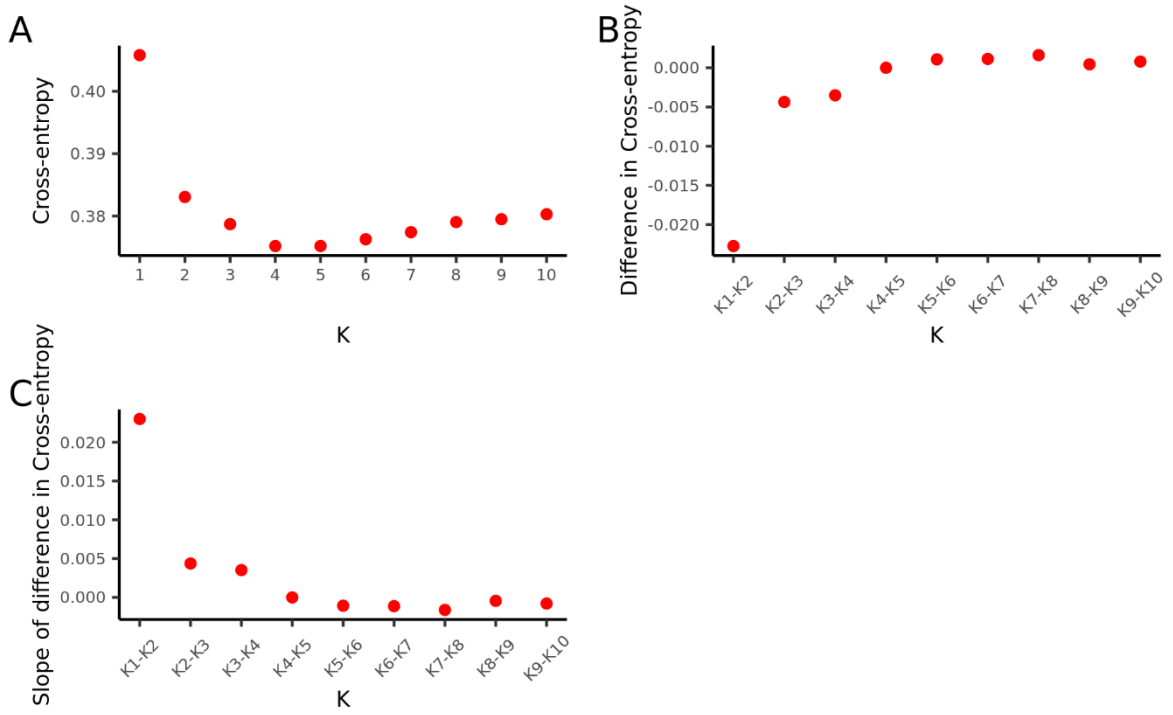

Figure 32. Cross-entropy (A), difference in Cross-entropy (B) and slope of difference in Cross-entropy (C).

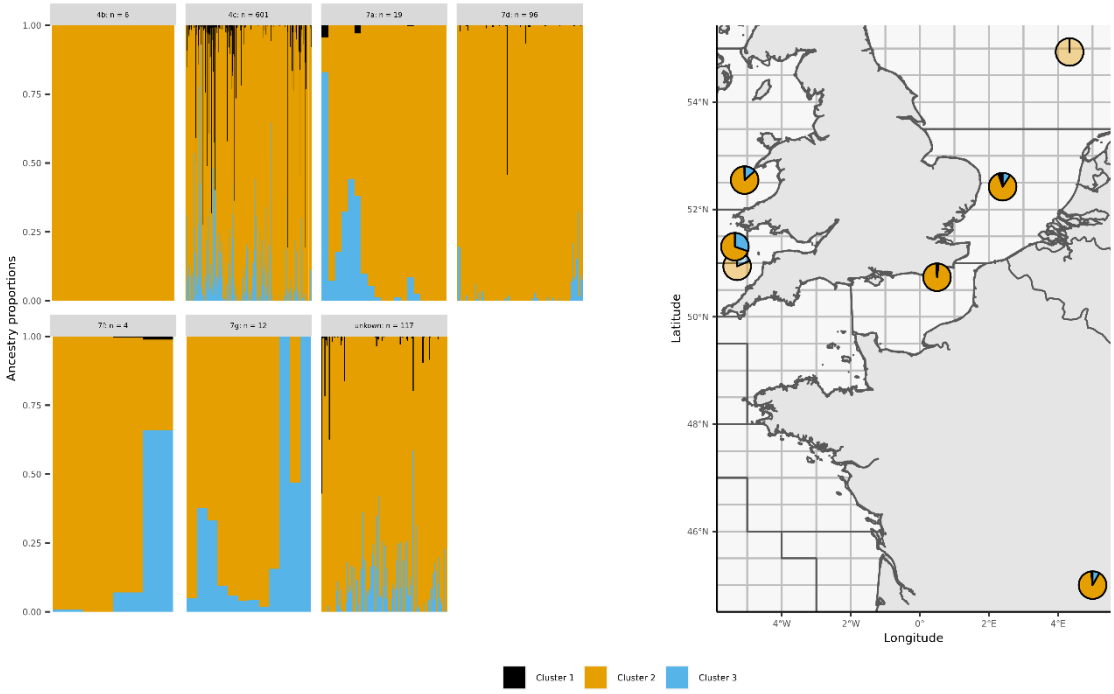

Figure 33. Ancestry proportions per sample (left) and average ancestry proportions by division (right) for K=3. Transparent pie charts indicate sub-populations with sample size < 10 samples. The pie chart in the South-East of France represents the combined 120 samples from the Greater North Sea ecoregions for which no clear spatial location could be determined.

Spotted ray

A total of 1200 samples of *Raja montagui* were collected and genotyped (Table 9Table). After quality control of samples and genotyped loci, 1049 samples remained for genetic population structure analyses (Table 9 & Figure 34).

Table 9. Initial and Postfiltering counts of Raja montagui by ecoregion and sex.

		Sample size		Sex	
Ecoregion	**Year**	**Initial**	**Post-filtering**	**No. of males**	**No. of females**
Greater North Sea	2004-2022	1,062	938	437	500
Greater North Sea (unkown location)	2019-2022	138	111	9	101
Total	2004-2022	1,200	1,049	446	601

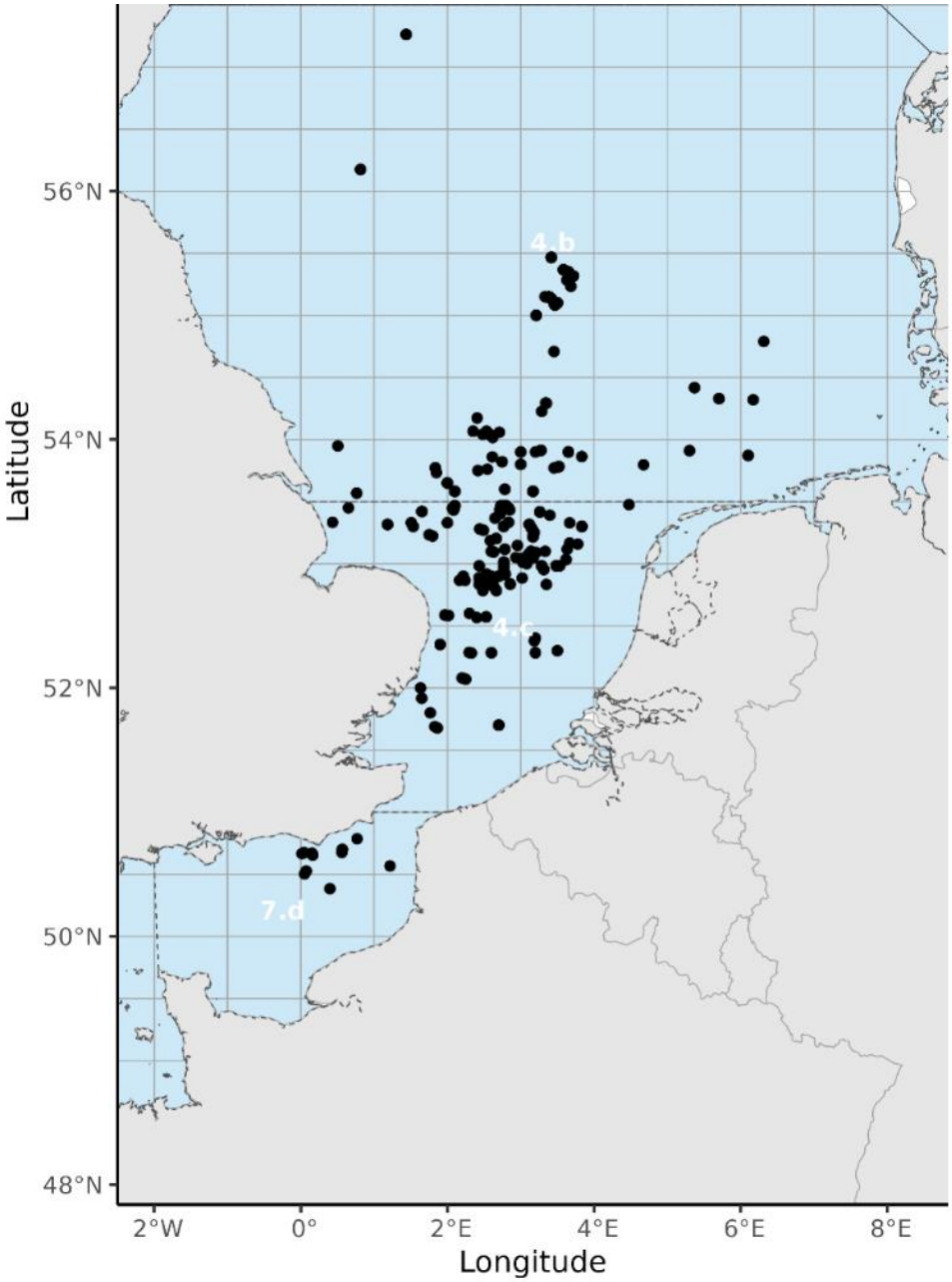

Figure 34. Spatial locations of 1049 Raja montagui samples analysed for genetic population structure.

Table 10. Summary of filtering steps for 1200 Samples and loci genotyped for Raja montagui.

Filtering Step	No. samples remaining	No. Loci remaining
Removed misidentified & duplicated samples, non-scoring loci, and monomorphic loci	1,200	97,702
Filter for loci reproducibility: ≥0.99	1,200	56,844
Loci call rate filter: ≥0.95	1,200	18,168
Remove secondary loci	1,200	13,121
Filter loci for read depth: lower limit ≥5, upper limit ≤50	1,200	12,558
Sample call rate filter: ≥0.95	1,138	10,478
Filter loci for minor allele frequency: ≥0.05	1,138	1,341
Remove unintentional Replicates	1,131	1,341
Remove sex-linked loci	1,131	1,337
Remove one loci of each loci pair in Linkage disequilibrium: >0.8	1,131	1,337
Remove one individual of each individual identified as first or second order kin pair	1,049	1,337

Here, a DAPC with ICES divisions was used as a grouping prior (Figure 35). A difference in clustering between samples in the Greater North Sea Ecoregion by ICES division was detected (Figure 37), when an optimal number of 148 PCs is used (Figure 36). Samples collected in 7d appear to cluster separate from 4b and 4c samples, indicating genetic population structure between the English Channel and the North Sea. An additional interesting observation is that many samples without spatial information provided, but likely fished in the North Sea, appear to cluster somewhat separately to samples collected in 4c and 4b.

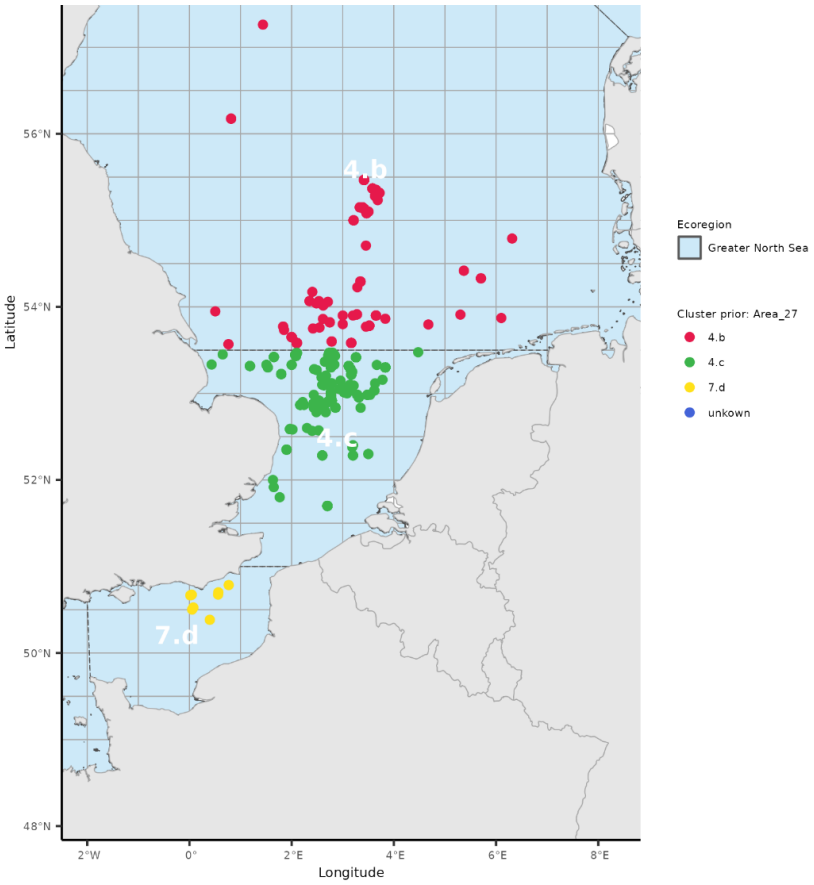

Figure 35. Spatial locations of 1049 Raja montagui samples colour coded by ICES division used as grouping prior for DAPC.

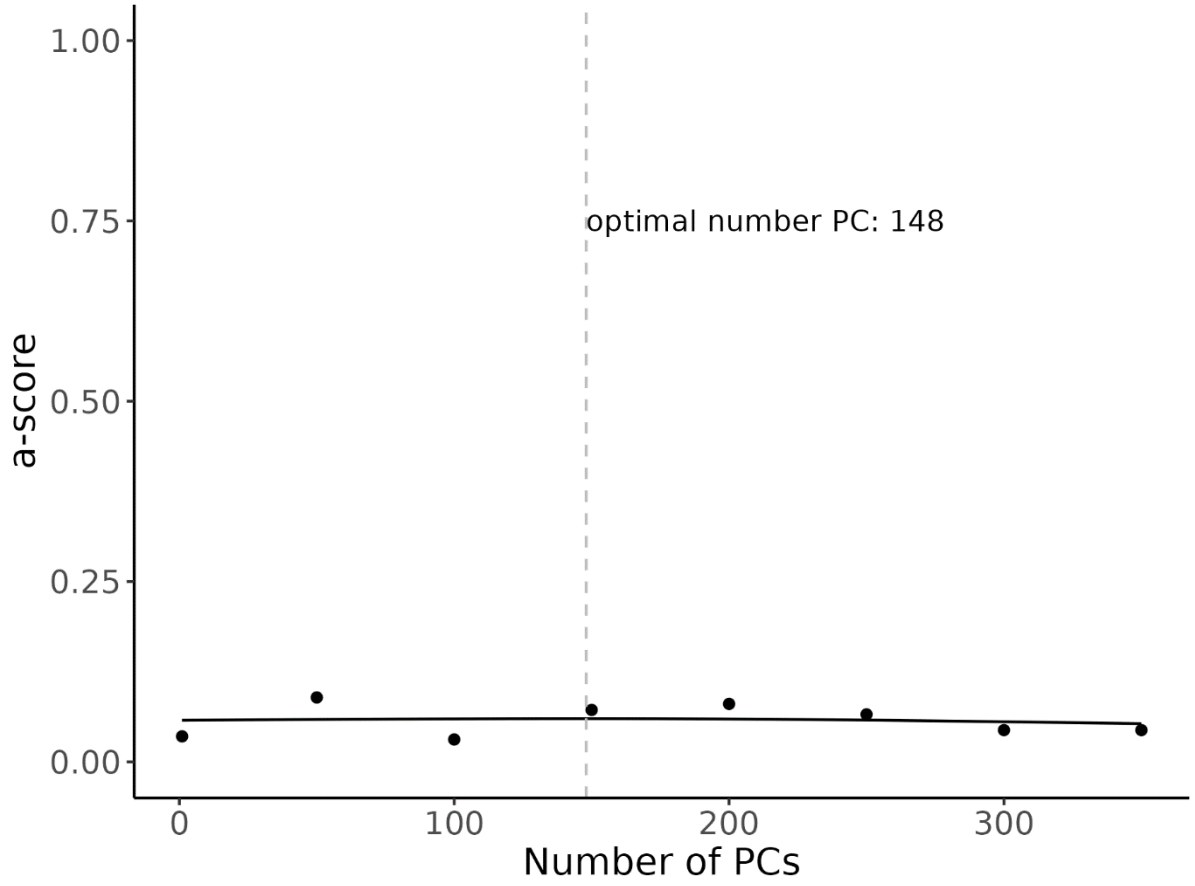

Figure 36. Estimated a-scores to determine optimal number of PCs to retain in DAPC with grouping Priors based on ICES division for Raja montagui.

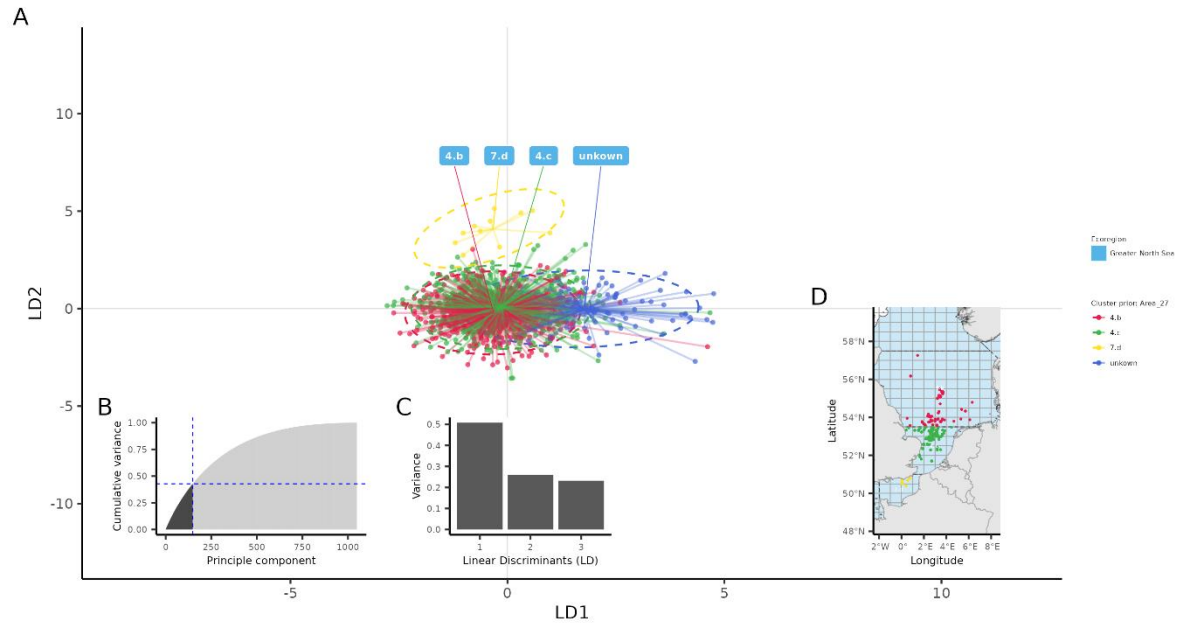

Figure 37. Discriminant analysis of principal components (DAPC) with grouping Prior based on ICES division (A). (B) Cumulative variance of 0.43 for optimal number of 148 PCs retained for DAPC. (C) Variance of linear discriminants retained in DAPC. (D) Sample locations of individuals colour coded by cluster results of DAPC.

The best DAPC model without prior grouping was the model with 1 cluster (K) as indicated by the lowest BIC (Figure 38). This suggests that no genetic population structure for *R. montagui* among the samples collected. As a DAPC requires K ≥2, results were investigated for DAPC without prior information for K≥2 and the best model K =3 was determined via the "elbow" in the difference of BICs and slope of difference of BICs (Figure 38) between subsequent clusters. For K = 3, the optimal number of Principal components (PCs) to retain in the DAPC is 115 (Figure 39), making up 0.35 of the cumulative variance observed, where LD1 explains >0.6 variance (Figure 40). A differentiation in the proposed 3 clusters can observed in the biplot of DAPC (Figure 41), however no population structure by spatial sampling locations across the Great North Sea is apparent (Figure 42).

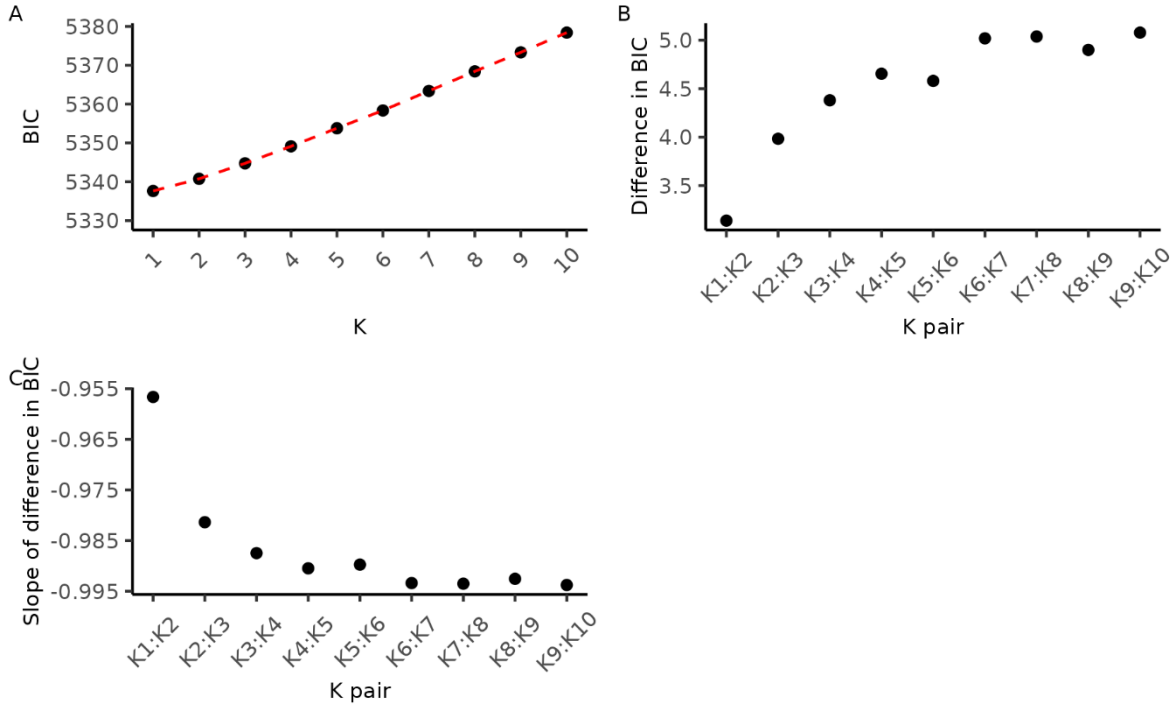

Figure 38. Cluster (K) evaluation of DAPC without prior grouping. (A) BIC for clusters, (B) Difference in BIC between clusters, and slope of difference between clusters.

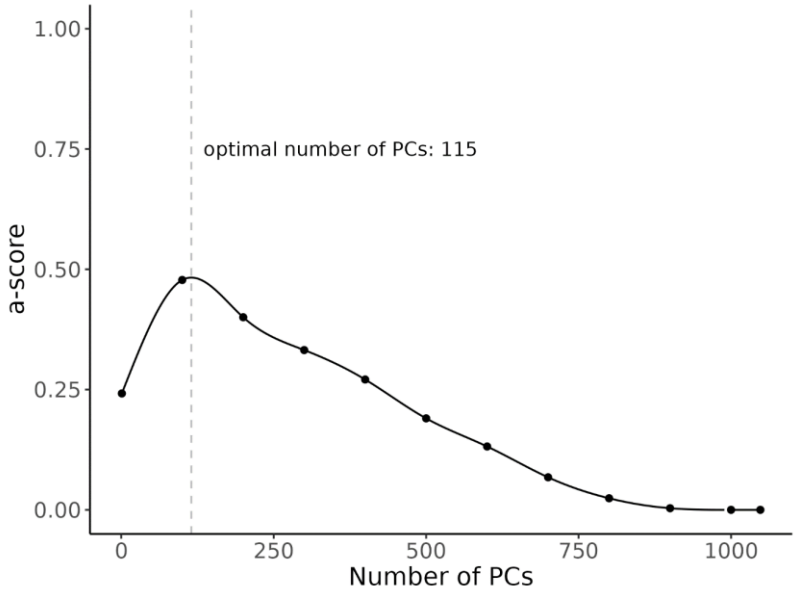

Figure 39. Estimated a-scores to determine optimal number of PCs to retain in DAPC without prior in K=3 for Raja montagui.

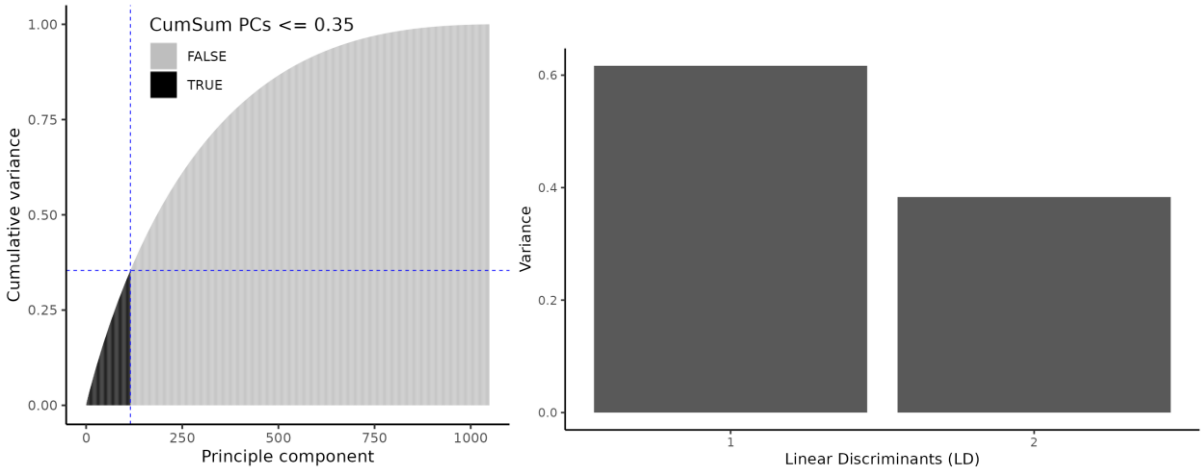

Figure 40. Cumulative variance of optimal number of 115 PCs retained for DAPC without prior in K=3 for Raja montagui.

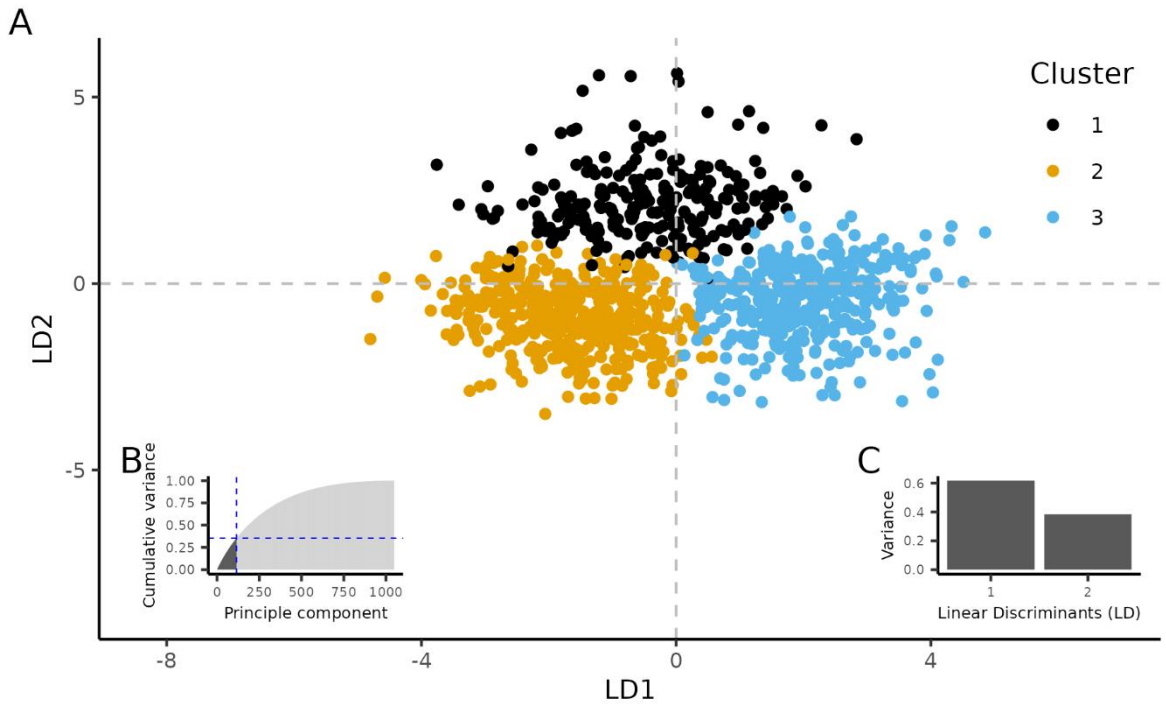

Figure 41. DAPC without prior for Raja montagui in K =3 (A), cumulative variance of optimal 115 PCs (B), and Variance of Linear Discriminants in the DAPC (C).

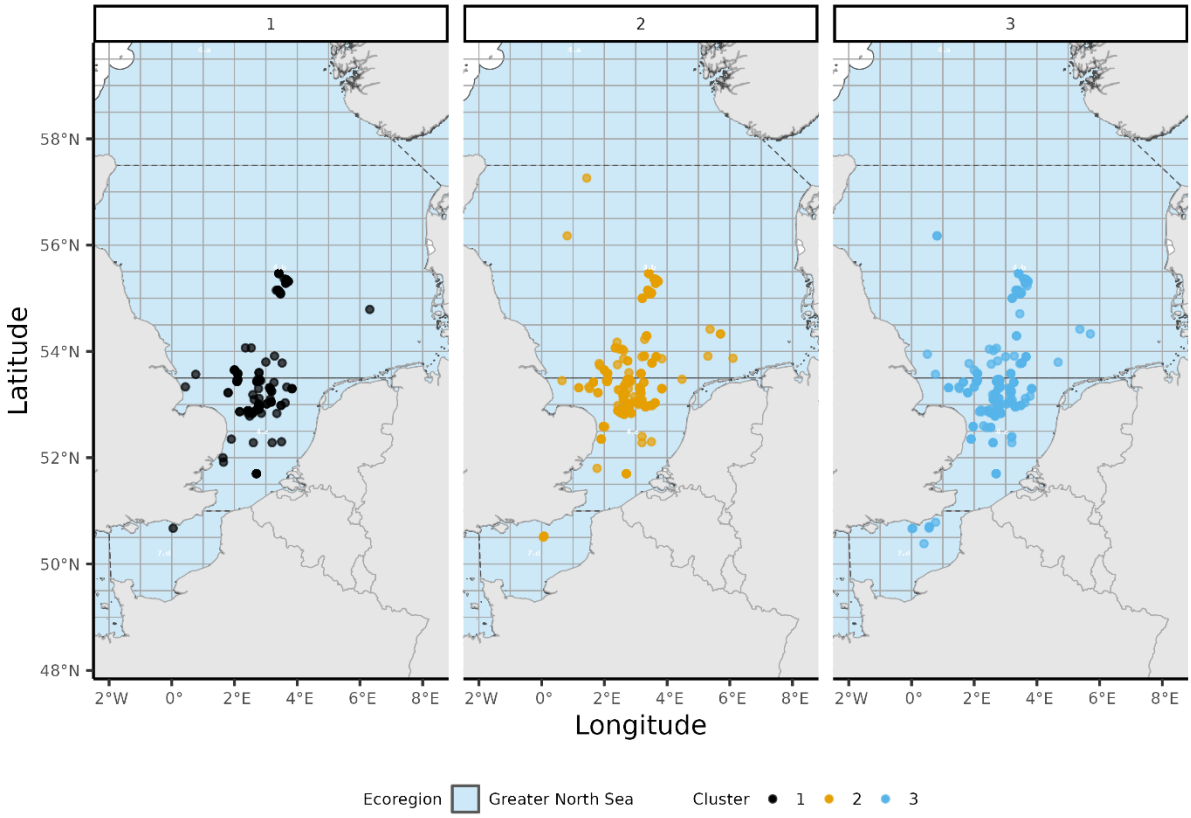

Figure 42. Samples of Raja montagui colour coded and facetted by clusters (K=3) detected by the DAPC without prior.

To study admixture the results are shown for the models with 2 clusters (K), as indicated by a lowest cross-entropy (Figure 43). Little population structure within the Greater North Sea ecoregion is apparent when plotting the average ancestral cluster proportions by ICES division (Figure 44) or by ices statistical rectangles (Figure 45), with only a slightly higher proportion of cluster 2 assigned to 4.b and 4.c (Figure 44).

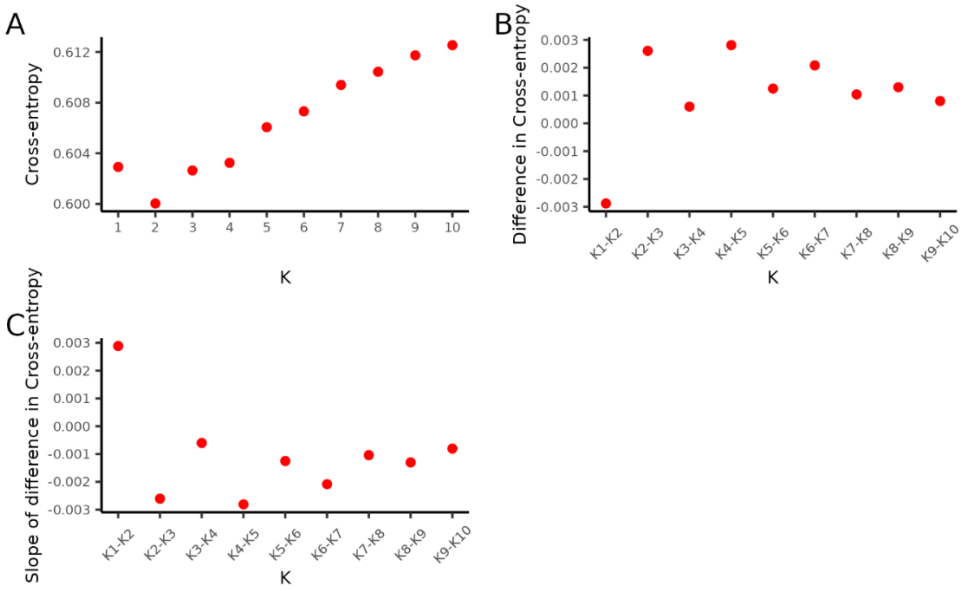

Figure 43. Cross-entropy (A), difference in Cross-entropy (B) and slope of difference in Cross-entropy (C).

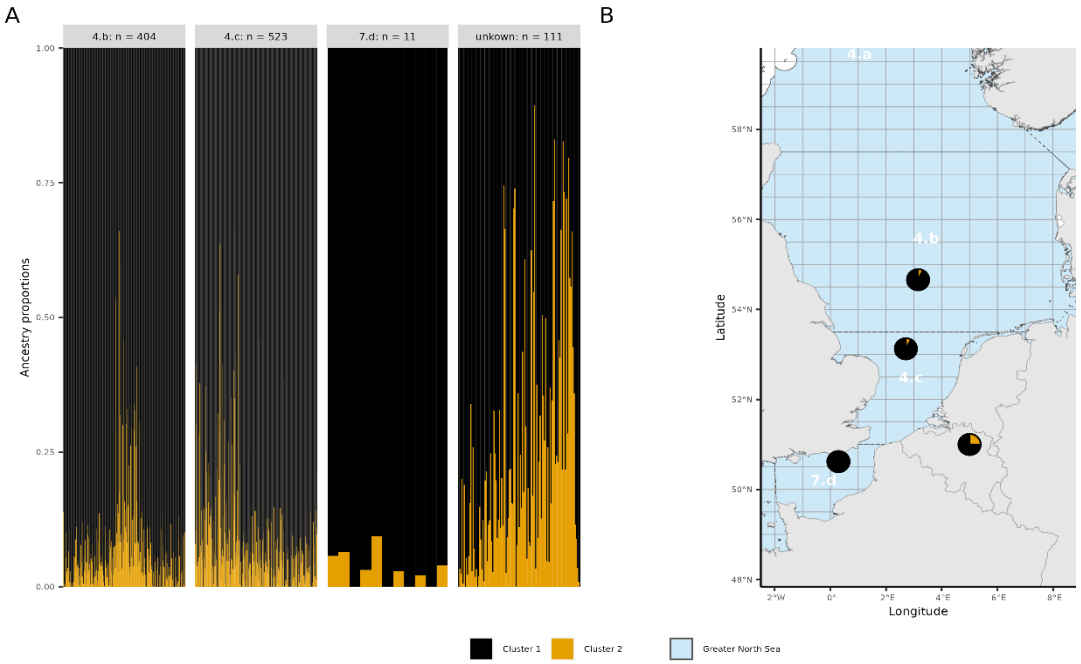

Figure 44. Ancestry proportions per sample (A) and average ancestry proportions by division(B) for K=2. Transparent pie charts indicate sub-populations with sample size < 5 samples. The pie chart in on the Netherlands represents the combined 111 samples from the Greater North Sea ecoregions for which no spatial location could be determined.

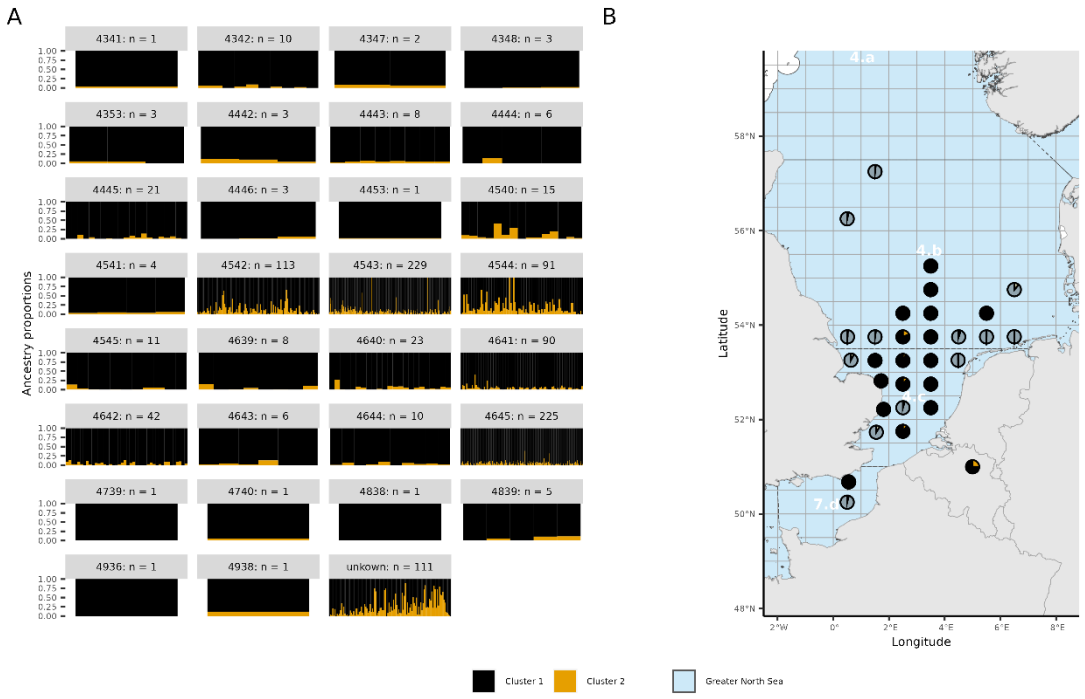

Figure 45. Ancestry proportions per sample (A) and average ancestry proportions by ICES statistical rectangle in the Greater North Sea (B) for K=2. Transparent pie charts indicate sub-populations with sample size < 5 samples. The pie chart in on the Netherlands represents the combined 111 samples from the Greater North Sea ecoregions for which no spatial location could be determined.

Discussion

While not yet complete, the tagging program in the project can be considered a success: of 224 released tags, 27 have yielded useful data to establish migration. There was a return rate of more than 13%, with many tags being returned from beaches. This return rate will only increase, because the first pop-off date will occur later this year. It is expected that after this date, a large number of tags will be returned through beach finds. These tags will have been deployed for over a year, revealing any annual migration pattern.

The current recaptures from fisheries, with known recapture locations do show that at least some individuals migrate large distances, with one individual crossing the North Sea between the Dutch and English coats, and several individuals crossing the boundaries of ICES divisions within the greater North Sea ecoregion. Future analyses of the depth and temperature stored on the tags will shed further light on these migration patterns, that can then be related to habitat use (Grubbs, 2010; Thorburn et al., 2019).

The depth data on the tags has already revealed daily vertical migration in *R. brachyura* and *R. montagui*, with rays generally staying near the bottom during day time, and making excursions into the water column at night, in line with earlier observations (Humphries et al. 2016). The effect of seasonal changes in the duration of daylight is yet to be studied, once the tags that are to pop-off are returned.

The analyses of survey data revealed a range extension of the populations of *R. clavata* and *R.brachyura.* Both species have increased in abundance in the Eastern English Channel and the Southern North Sea. For *R. clavata*, at the start of our observations located off the English coast in the southern North Sea and Eastern English Channel, we now observe an extension of this distribution, north of the Netherlands. For *R. brachyura*, we observe a similar extension in the southern North Sea. This species was previously considered as having two stocks in the greater North Sea Ecoregion: one in ICES Subarea 6 and ICES Division 4a, and one in ICES Divisions 4c and 7d (ICES 2018). Hence, catches of *R. brachyura* could not be allocated to a stock. During an ICES benchmark on elasmobranch stocks in 2023 (ICES 2023), the results of the analyses of survey data were presented, leading to the addition of ICES Divisions 4b to the ICES Divisions 4c and 7d stock.

No clear population genetic structure was observed within the Greater North Sea ecoregion for any of the three stocks. In contrast, clear population structure was found within the Bay of Biscay, where differences were found between inidviduals from the shallow coast and those from deeper waters further offshore (Trenkel et al., 2022).

The large number of genotypes collected in different programs over the years, including this program, can also be used for inferring population size based on Close-Kin Mark-Recapture (Bravington et al. 2016; Hillary et al., 2018). In a previous study on *R. clavata (*Poos et al., 2022*)*, a limited number of half-sibling pairs were found. The newly collected genotypes revealednew half-sibling pairs that can be used in the future for abundance estimation based on CKMR.

To conclude, there are clear increases observed in the abundances of the demersal elasmobranch stocks in the Southern part of the Greater North Sea ecoregion. As a result, more rays are observed in the Dutch part of the North Sea. Meanwhile, no clear population genetic structure was observed for the stocks. This could be explained by the migration that is observed from tagging data, even with the limited set of tags that has yet been returned. The tags that have been returned show clear diel vertical migration patterns in all species. The number of returned tags is expected to increase substantially over the next two years, as more pop-off dates are reached. Such a full set of tag data can be used to reconstruct annual migration patterns, as was demonstrated by the tags analysed in this study.

.

Acknowledgements

This study would not have been possible without the efforts of countless researchers and fishers, who helped in tagging animals and in collecting samples aboard their vessels, or authorized the collection of samples. For this we are very grateful. Likewise, we want to thank all people returning tags after these were found on the beach. Finally, we would also like to express our gratitude to David Righton from CEFAS, who contributed to the analysis of the migration patterns for a limited set of tags. We are looking forward to further collaboration on analysing the full set of tags once we have retrieved a larger number of tags.

Literature

Anderson, E. C. (2022) CKMRsim: Inference of Pairwise Relationships Using Likelihood Ratios. R package version 0.1.1.999 edn.

Andrews, K.S., Williams, G.D., Farrer, D., Tolimieri, N., Harvey, Chris J., Bargmann, G., Levin, P.S. (2009) Diel activity patterns of sixgill sharks, Hexanchus griseus: the ups and downs of an apex predator. Animal Behaviour, 78(2): 525–536.

Amelot, M., Batsleer, J., Foucher, E., Girardin, R., Marchal P., Poos J. J., Sys K. (2021) Evidence of difference in landings and discards patterns in the English Channel and North Sea Rajidae complex fishery. Fisheries Research, 242: 106028.

Bird, C., Burt, G.J., Hampton, N., McCully Phillips, S.R., Ellis, J.R. (2020) Fifty years of tagging skates (Rajidae): Using mark-recapture data to evaluate stock units. Journal of the Marine Biological Association of the United Kingdom, 100(1): 121–131.

Bravington, M.V., Grewe, P.M., Davies, C.R. (2016) Absolute abundance of southern bluefin tuna estimated by close-kin mark-recapture. Nature Communications, 7: 13162.

Bresadola L., Link V., Buerkle C.A., Lexer C., Wegmann D. (2020) Estimating and accounting for genotyping errors in RAD-seq experiments. Molecular Ecology Resources, 20: 856– 870.

Brevé, N.W.P., Winter, H.V., Wijmans, P.A.D.M., Greenway, E.S.I., Nagelkerke, L.A.J.(2020) Sex differentiation in seasonal distribution of the starry smooth-hound Mustelus asterias. Journal of Fish Biology, 97(6): 1870–1875.

Di Santo, V., Kenaley, C.P., Lauder, G.V. (2017) High postural costs and anaerobic metabolism during swimming support the hypothesis of a U-shaped metabolism–speed curve in fishes. Proceedings of the National Academy of Sciences of the United States of America, 114: 13048–13053.

Dulvy, N.K., Metcalfe, J.D., Glanville, J., Pawson, M.G., Reynolds, J.D. (2000) Fishery stability, local extinctions, and shifts in community structure in skates. Conservation Biology, 14: 283-2.

Elshire, R.J., Glaubitz, J.C., Sun, Q., Poland, J., Kawamoto, K., Buckler, E.S., Mitchell, S.E. (2011) A robust, simple genotyping-by-sequencing (GBS) approach for high diversity species. PLoS ONE, 6(5): e19379.

Frichot, E., Mathieu, F., Trouillon, T., Bouchard, G., Francois, O. (2014) Fast and efficient estimation of individual ancestry coefficients. Genetics, 196: 973-983.

Frisk, M.G., Miller, T.J., Fogarty, M.J. (2001) Estimation and analysis of biological parameters in elasmobranch fishes: A comparative life history study. Canadian Journal of Fisheries and Aquatic Sciences, 58: 969-981.

Greenway, E., Jones, K.S., Cooke, G.M. (2016) Environmental enrichment in captive juvenile thornback rays, Raja clavata (Linnaeus 1758). Applied Animal Behaviour Science, 182: 86-93.

Grubbs, R.D. (2010) Ontogenetic shifts in movements and habitat use. Sharks and Their Relatives II: Biodiversity, Adaptive Physiology, and Conservation, pp. 319–350

Heithaus, M.R., Frid, A. Wirsing, A.J., Worm, B. (2008) Predicting ecological consequences of marine top predator declines. Trends in Ecology & Evolution, 23(4): 202-210.

Hillary, R.M., Bravington, M.V., Patterson, T.A., et al. (2018) Genetic relatedness reveals total population size of white sharks in eastern Australia and New Zealand. Scientific Reports, 8(1):2661.

Humphries, N.E., Simpson, S.J., Sims, D.W. (2017) Diel vertical migration and central place foraging in benthic predators. Marine Ecology Progress Series, 582: 163–180.

Hunter, E., Buckley, A.A., Stewart, C., Metcalfe, J.D. (2005) Migratory behaviour of the thornback ray, Raja clavata, in the southern North Sea. Journal of the Marine Biological Association of the United Kingdom, 85: 1095-1105.

ICES (2018) Report of the Working Group on Elasmobranch Fishes (WGEF), 19–28 June 2018, Lisbon, Portugal. ICES CM 2018/ACOM:16. 1306 pp.

ICES (2021) ICES Database of Trawl Surveys (DATRAS), Extraction 13 February 2021, International Bottom Trawl Survey (IBTS), Beam Trawl Survey (BTS) and French Groundfish Channel Survey (FR-CGFS). Copenhagen.

ICES. (2023) Benchmark workshop on selected elasmobranch stocks (WKBELASMO). ICES Scientific Reports. 5:45. 117 pp. http://doi.org/10.17895/ices.pub.22760042

Jombart, T., Devillard, S., Balloux, F. (2010) Discriminant analysis of principal components: a new method for the analysis of genetically structured populations. BMC Genetics, 11: 94.

Jona Lasinio, G., Mastrantonio, G., Pollice, A. (2012) Discussing the "big n problem". Statistical Methods & Applications, 22: 97-112.

Kilian, A., Wenzl, P., Huttner, E., Carling, J., Xia, L., Blois, H., Caig, V., Heller-Uszynska, K., Jaccoud, D., Hopper, C., Aschenbrenner-Kilian, M., Evers, M., Peng, K., Cayla, C., Hok, P., & Uszynski, G. (2012) Diversity Arrays Technology: A generic genome profiling technology on open platforms. Methods in Molecular Biology, 888: 67– 89.

Lezama-Ochoa, N., Pennino, M. G., Hall, M. A., Lopez, J., Murua, H. (2020) Using a Bayesian modelling approach (INLA-SPDE) to predict the occurrence of the Spinetail Devil Ray (Mobular mobular). Scientific Reports, 10: 18822.

Marandel F., Charrier G., Lamy J.-B., Le Cam S., Lorance P., Trenkel V. M. (2020) Estimating effective population size using RADseq: effects of SNP selection and sample size. Ecology and Evolution, 10: 1929–1937.

McCully, S.R., Scott, F., Ellis, J.R., (2012) Lengths at maturity and conversion factors for skates (Rajidae) around the British Isles, with an analysis of data in the literature. ICES Journal of Marine Science, 69: 1812-1822.

Mehner, T., Kasprzak, P., Hölker, F. (2007) Exploring ultimate hypotheses to predict diel vertical migrations in coregonid fish. Canadian Journal of Fisheries and Aquatic Sciences, 64(6): 874–886.

Mehner, T. (2012) Diel vertical migration of freshwater fishes - proximate triggers, ultimate causes and research perspectives. Freshwater Biology, 57(7): 1342–1359.

Pennino, M. G., Muñoz, F., Conesa, D., López-Quilez, A., Bellido, J. M. (2013) Modeling sensitive elasmobranch habitats. Journal of Sea Research, 83: 209-218.

Poos, J.J., Staudle, T. Megens, H. J. (2022) Genetische analyses voor stekelrog en blonde rog.Wageningen University and Research report. https://edepot.wur.nl/582408.

Raj, A., Stephens, M., Pritchard, J.K. (2014) FastSTRUCTURE: Variational inference of population structure in large SNP data sets. Genetics, 197: 573-589.

Roos, M., Held, L. (2011) Sensitivity analysis in Bayesian generalized linear mixed models for binary data. Bayesian Analysis, 6: 259-278.

Rue, H., Martino, S., Chopin, N. (2009) Approximate Bayesian inference for latent Gaussian models by using integrated nested Laplace approximations. Journal of the Royal Statistical Society (Series B) 71: 319-392.

Shepard, E.L.C., Ahmed, M.Z., Southall, E.J., Witt, M.J., Metcalfe, J.D., Sims, D.W. (2006) Diel and tidal rhythms in diving behaviour of pelagic sharks identified by signal processing of archival tagging data. Marine Ecology Progress Series, 328: 205–213.

Sims, D.W., Witt, M.J., Richardson, A.J., Southall, E.J., Metcalfe, J.D. (2006) Encounter success of free-ranging marine predator movements across a dynamic prey landscape. Proceedings of the Royal Society B: Biological Sciences, 273; 1195-1201.

Sims, D.W., Wearmouth, V.J., Southall, E.J., Hill, J.M., Moore, P., Rawlinson, K., Hutchinson, N., Budd, G.C., Righton, D., Metcalfe, J.D., Nash, J.P., Morritt, D. (2006) Hunt warm, rest cool: Bioenergetic strategy underlying diel vertical migration of a benthic shark. Journal of Animal Ecology, 75: 176-190.

Sguotti, C., Lynam, C.P., García-Carreras, B., Ellis, J.R., Engelhard, G.H. (2016) Distribution of skates and sharks in the North Sea: 112 years of change. Global change biology, 22: 2729-2743.

Thorburn, J., Neat, F., Burrett, I., Henry, L.-A., Bailey, D. M., Jones, C.S., Noble, L.R.(2019) Ontogenetic variation in movements and depth use, and evidence of partial migration in a benthopelagic elasmobranch. Frontiers in Ecology and Evolution, 7: 353

Thorson, J. T., Minto, C. (2015) Mixed effects: a unifying framework for statistical modelling in fisheries biology. ICES Journal of Marine Science, 72: 1245-1256.

Trenkel, V. M., Boudry, P., Verrez-Bagnis, V., and Lorance, P. (2020) Methods for identifying and interpreting sex-linked SNP markers and carrying out sex assignment: application to thornback ray (Raja clavata). Molecular Ecology Resources, 20: 1610– 1619.

Trenkel, V.M., Charrier, G., Lorance, P., Bravington, M.V. (2022) Close-kin mark-recapture abundance estimation: Practical insights and lessons learned. ICES Journal of Marine Science, 79: 413-422.

Walker, P. A., Heessen, H. J. L. (1996). Long-term changes in ray populations in the North Sea. ICES Journal of Marine Science, 53(6): 1085-1093.

Walker, P. A. (1999) Fleeting images: dynamics of North Sea ray populations. University of Amsterdam.

Walker, N. D., Maxwell, D. L., Le Quesne, W. J. F., Jennings, S. (2017) Estimating efficiency of survey and commercial trawl gears from comparisons of catch-ratios. ICES Journal of Marine Science, 74: 1448-1457.

Appendix A

Sampling Protocol finclips rays and skates

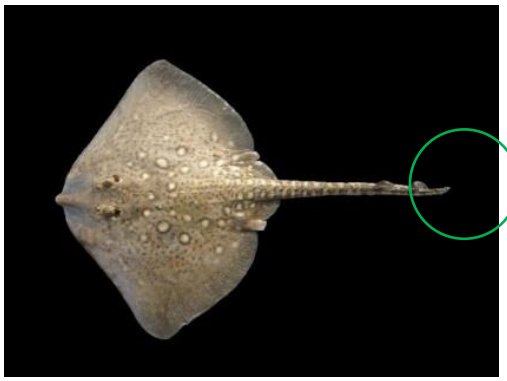

Figure A1 Location of dorsal fins

Material:

Measuring board
Scale (not compulsory)
Gloves
2 ml tubes filled with 70% pure ethanol
Scissors
Tweezers

Method:

1) Provide geographic location of catch, as precisely as possible
2) Determine of the sex of the fish
3) Measure Total Length (TL) to the lower nearest cm
4) Where possible, measure the weight of the fish
5) Additional (not compulsory data): determine maturity stage

Sampling

Gloves may be used but are not mandatory. Rinse tweezers and scissors with tap or sea water between each fish(1). Cut a small piece of the dorsal fins(2) using tweezers and scissors. Store the samples in a pre-filled tube (photo). Tubes are pre-labeled and corresponding data are to be recorded on the provided form.

(1) The sampling needs to be done in domestic clean condition, e.g. like for cooking, but not strictly like "white lab" or "clean lab" conditions.

(2) Rays can be released alive, we already had ray sampled in this way, that were tagged and recaptured.

Storage of samples

Store samples at -20 °C and transport in cooler with ice.

Thank

Figure A2 Example of 2 ml tube containing a sample of dorsal fin